High-resolution vertical biogeochemical profiles in the hyporheic zone reveal insights into microbial methane cycling

Tamara Michaelis[1], Anja Wunderlich[1], Ömer K. Coskun[2], William Orsi[2,3], Thomas Baumann[1], Florian Einsiedl[1]

[1] Chair of Hydrogeology, School of Engineering and Design, Technical University Munich, Munich, Germany
[2] Department of Earth and Environmental Sciences, Paleontology & Geobiology, Ludwig-Maximilians-Universität München, 80333 Munich, Germany.
[3] GeoBio-Center[LMU], Ludwig-Maximilians-Universität München, 80333 Munich, Germany

Correspondence to: Florian Einsiedl (f.einsiedl@tum.de)

Abstract. Facing the challenges of climate change, policy making relies on sound greenhouse gas (GHG) budgets. Rivers and streams emit large quantities of the potent GHG methane (CH_4), but their global impact on atmospheric CH_4 concentrations is highly uncertain. In-situ data from the hyporheic zone (HZ), where most CH_4 is produced and some of it can be oxidized to CO_2, are lacking for an accurate description of CH_4 production and consumption in streams. To address this, we recorded high-resolution depth-resolved geochemical profiles at five different locations in the stream bed of river Moosach, Southern Germany. Specifically, we measured pore-water concentrations and stable carbon isotopes ($\delta^{13}C$) of dissolved CH_4 as well as relevant electron acceptors for oxidation with a 1 cm vertical depth-resolution. Findings were interpreted with the help of a numerical model, and 16S rRNA gene analyses added information on the microbial community at one of the locations. Our data confirms with pore-water CH_4 concentrations of up to 1000 µmol L^{-1} that large quantities of CH_4 are produced in the HZ. Stable isotope measurements of CH_4 suggest that hydrogenotrophic methanogenesis represents a dominant pathway for CH_4 production in the HZ of river Moosach, while a relatively high abundance of a novel group of methanogenic archaea, the Methanomethyliales (Phylum Verstraetearchaeota), indicate that CH_4 production through H_2 dependent methylotrophic methanogenesis might also be an important CH_4 source. Combined isotopic and modeling results clearly implied CH_4 oxidation processes at one of the sampled locations, but due to the steep chemical gradients and the close proximity of the oxygen and nitrate reduction zones no single electron acceptor for this process could be identified. Nevertheless, the numerical modeling results showed not only a potential for aerobic CH_4 oxidation, but also for anaerobic oxidation of CH_4 coupled to denitrification. In addition, the nitrate-methane transition zone was characterized by an increased relative abundance of microbial groups (*Crenothrix*, NC10) known to mediate nitrate and nitrite dependent methane oxidation in the hyporheic zone. This study demonstrates substantial CH_4 production in hyporheic sediments, a potential for aerobic and anaerobic CH_4 oxidation and underlines the high spatiotemporal variability of this habitat.

1 Introduction

At the UN Climate Change conference 2021 (COP26) in Glasgow over 100 countries signed the Global Methane Pledge, an agreement to reduce CH_4 emissions by 30 % until 2030 compared to 2020 levels (European Commission and United States of America, 2021). CH_4 has been estimated to account for 20 % of the Earth's warming (Kirschke et al., 2013) and atmospheric methane concentrations have increased with a significant acceleration in recent years (Nisbet et al., 2019). The largest source of uncertainty in global CH_4 budgets are natural emissions (Saunois et al., 2020). Although rivers and streams represent only a small fraction of surface waters, they contribute considerable amounts of CH_4 to atmospheric concentrations (Saunois et al., 2020). Based on the evaluation of 385 globally distributed sites, rivers and streams are expected to emit 27 Tg CH_4 y^{-1} (Stanley et al., 2016) which is equal to 756 Tg CO_2 equivalents (IPCC, 2013) and constitutes approximately 17 % of freshwater emissions and 7 % of all natural sources (Saunois et al., 2020).

In rivers and streams CH_4 production is a microbially driven process concentrated in anaerobic sediments of the hyporheic zone (HZ) (Trimmer et al., 2012). The HZ represents a spatially and temporarily dynamic saturated subsurface layer where stream water enters a river's bed and banks and is a zone known for high biogeochemical activity (Findlay, 1995; Winter et al., 1998). Hyporheic exchange delivers electron acceptors such as oxygen (O_2), nitrate (NO_3^-), sulfate (SO_4^{2-}), as well as nutrients and organic carbon (OC) to the HZ where microbially mediated transformation reactions take place (Boano et al., 2014). After dissolved O_2 is consumed, other terminal electron acceptors become dominant in consecutive zones of denitrification, mangangese (Mn)-, iron (Fe)- and SO_4^{2-} reduction and finally, CH_4 production (methanogenesis) (Canfield and Thamdrup, 2009).

CH_4 is produced by methanogens, strictly anaerobic archaea that thrive where the environment is deprived of light, NO_3^- and SO_4^{2-} (Deppenmeier, 2002). Two metabolic pathways dominate CH_4 production in natural environments, hydrogenotrophic and acetoclastic methanogenesis (Conrad, 2005). Diffusing upwards from anaerobic sediments, CH_4 can be oxidized to CO_2 by methanotrophic microorganisms before reaching the atmosphere. The most abundant methanotrophs are aerobic methanotrophic Proteobacteria (Nazaries et al., 2013), but when the environment is depleted in O_2, other electron acceptors such as NO_3^- and NO_2^- can be utilized in anaerobic oxidation of methane (AOM). Archaea from the ANME-2d clade like *Candidatus* Methanoperedens nitroreducens (*M. nitroreducens*) couple NO_3^- reduction with CH_4 oxidation (Haroon et al., 2013; Arshad et al., 2015). Bacteria of the genus *Candidatus* Methylomirabilis of the NC10 phylum use NO_2^- as electron acceptor (Ettwig et al., 2010; Graf et al., 2018; Versantvoort et al., 2018; He et al., 2016). Oswald et al. (2017) and Kits et al. (2015) found indications that *Crenothrix* and *Methylomonas denitrificans* are facultative anaerobic methanotrophs consuming NO_3^- in O_2 depleted environments. Methane oxidation coupled to denitrification has been shown to occur in many freshwater environments including lakes (Einsiedl et al., 2020; Graf et al., 2018; Deutzmann et al., 2014; Oswald et al., 2017; Norði and Thamdrup, 2014; Peña Sanchez et al., 2022), reservoirs (Naqvi et al., 2018) and wetlands (Hu et al., 2014; Zhang et al., 2018; Zhu et al., 2015; Shen et al., 2017). AOM can also be coupled to the reduction of sulfate (S-DAMO) and the metals Fe and Mn (M-DAMO) (Beal et al., 2009; Reeburgh, 1976). Evidence has accumulated that S-DAMO occurs in freshwater habitats

(Van Grinsven et al., 2020; Eller et al., 2005; Schubert et al., 2011; Norði et al., 2013; Segarra et al., 2015; Timmers et al., 2016; Ng et al., 2020) despite the low energy yield and typically low SO_4^{2-} concentrations.

Several recent studies have addressed the question which predictors best explain the spatiotemporal variability of methanogenesis and CH_4 oxidation in rivers and streams. For example, Shen et al. (2019) compared potential AOM activity in different river sediments under laboratory conditions and found that the addition of NO_3^-, NO_2^-, SO_4^{2-} and Fe^{3+} could provoke AOM activity in sandy river beds, while no AOM could be stimulated in gravelly river beds. This is in line with findings by Shelley et al. (2015) and Bodmer et al. (2020) who measured increasing CH_4 production and oxidation capacity with decreasing grain diameter. Other parameters stimulating CH_4 production and oxidation in streams are high organic carbon contents (Bodmer et al., 2020; Romeijn et al., 2019; Bednařík et al., 2019; Crawford et al., 2017) and shading (Shelley et al., 2017). Further, methanogenic and methanotrophic activity in river sediments has been found to increase with rising temperature (Shelley et al., 2015; Comer-Warner et al., 2018).

While all these studies quantified potential CH_4 production and oxidation rates in laboratory incubation experiments, only few studies have measured vertical geochemical gradients on-site to investigate the depth-distribution of redox zones in stream beds in the context of CH_4 cycling. Exceptions are for example the work of Villa et al. (2020) who measured vertical profiles of CH_4, CO_2 and N_2O at different beach positions and water stages to examine the relation of hyporheic exchange and GHG emissions, and Ng et al. (2020) who showed that S-DAMO could reduce CH_4 concentrations in a wetland-stream system by interpreting vertical geochemical profiles with a multicomponent reactive transport model. Yet, spatial patterns of methanogenic and CH_4 oxidation zones in the HZ remain largely unexplored. Therefore, more field data are required to accurately describe how much CH_4 is produced and consumed in streams, and under which conditions.

Attempting to fill this knowledge gap, we measured high-resolution depth-resolved geochemical profiles at different locations in a stream bed to study the spatial patterns of CH_4 production and oxidation and to investigate the potential for AOM. As our study site we chose the HZ of a stream dominated by fine, organic-rich sediments that has a high potential to form and emit substantial amounts of CH_4. To support the interpretation of vertical concentration profiles of O_2, NO_3^-, NO_2^-, SO_4^{2-} and CH_4 we measured stable carbon-isotopes of CH_4. In addition, quantitative PCR and sequencing of 16S rRNA genes were performed on a sediment core at one of the locations. The 1D numerical modeling software PROFILE (Berg et al., 1998) was used to support the interpretation of the measured geochemical profiles.

2 Materials and methods

2.1 Site characterization and determination of sediment properties

Five different sites in the hyporheic zone of river Moosach in Southern Germany were chosen for the sampling campaigns in 2020 and 2021. River Moosach is a groundwater fed stream with a topographic catchment area of 175 km^2 which originates in two moor drainage ditches north of the city of Munich and runs along the border of two contrasting geological landscapes, the Tertiary Hill Country on the left and the Munich Gravel Plain on the right bank (Pulg et al., 2013; Auerswald and Geist,

2018). The river water can be characterized as a calcium-magnesium-bicarbonate type with elevated concentrations of chloride. Stream water chemistry is further characterized in Appendix A. Upstream of the points of measurement, the river crosses the 'Freisinger Moos', a heavily drained lowland moor area (Zehlius-Eckert et al., 2003). Human activities like damming, diversions and straightening measures have significantly altered the natural course and hydrological behavior of the Moosach since the Middle Ages (Pulg et al., 2013). The discharge is controlled by weirs and check dams leading to stable hydrologic conditions. Impoundments nowadays constitute about one third of the river's length leading to a decreased gradient, flow velocity and shear stress (Pulg et al., 2013). The Moosach river is subject to colmation and siltation, 51 % of the gravel bed is covered with fine deposits (Auerswald and Geist, 2018). Auerswald and Geist (2018) performed an extensive study on the composition of these fine deposits in river Moosach and found that on average 46 % were carbonates dominated by calcite, 38 % silicates and 16 % organic matter. Macrophytes cover approximately 15 % of the river bed which decreases average flow velocity due to increased hydraulic roughness (Braun et al., 2012). Braun et al. (2012) found average flow velocities above ground of 0.11 m s^{-1} and 0.16 m s^{-1} in cross sections with and without macrophytes, respectively.

The sampling sites are situated in the middle section of the river where the energy slope drops below the average of 1.3 ‰ to as low as 0.1 ‰ in some places and where fine deposits predominate (Auerswald and Geist, 2018). Stream water temperatures as recorded at a monitoring station of the Bavarian State Office of the Environment 4.5 km downstream of the sampling sites lie on average between 6.2 °C in January and 16.3 °C in July. The annual mean discharge of the Moosach is 2.46 m^3 s^{-1}, low flow conditions generally prevail between July and September and high flow events are more common in winter and spring. Detailed information on stream discharge and surface water temperatures during the sampling period is given in Fig. 1.

A schematic map of the five sampling locations and their placement in the river cross section is given in Figure 2a and b. At this section, river Moosach is typically 10-12 m wide with a maximum water depth of approximately 1.3-1.4 m. At each site, a geochemical pore water profile was recorded as described in Sec. 2.2 and sediment grain size distributions were determined. Additionally, basic chemical parameters of the surface water (temperature, dissolved oxygen concentration, pH and electrical conductivity) were measured at each sampling day. For location C, an additional sediment core was taken for microbiological analyses.

Detailed information on sampling periods, surface water chemistry and sedimentary composition of each sampling site is given in Appendix A. In short, at each site a high-resolution geochemical profile was measured with an equilibrium dialysis sampler (peeper) which remained in the sediment for at least three weeks. Sediment composition was analyzed with sieve-slurry analyses following the DIN EN ISO 17892-4 standard (Fig. A1). With 65-75 % silt and clay, the most fine-grained material is found at the right banks at locations A and E. At the outside bend of the right bank (location B) a clear stratification was found with gravel between 0-11 cm depth and sandy silt below. Deposits at location C consisted of 60-63 % silt and clay. At location D, central in the river, sand had the main fraction with 66-79 %.

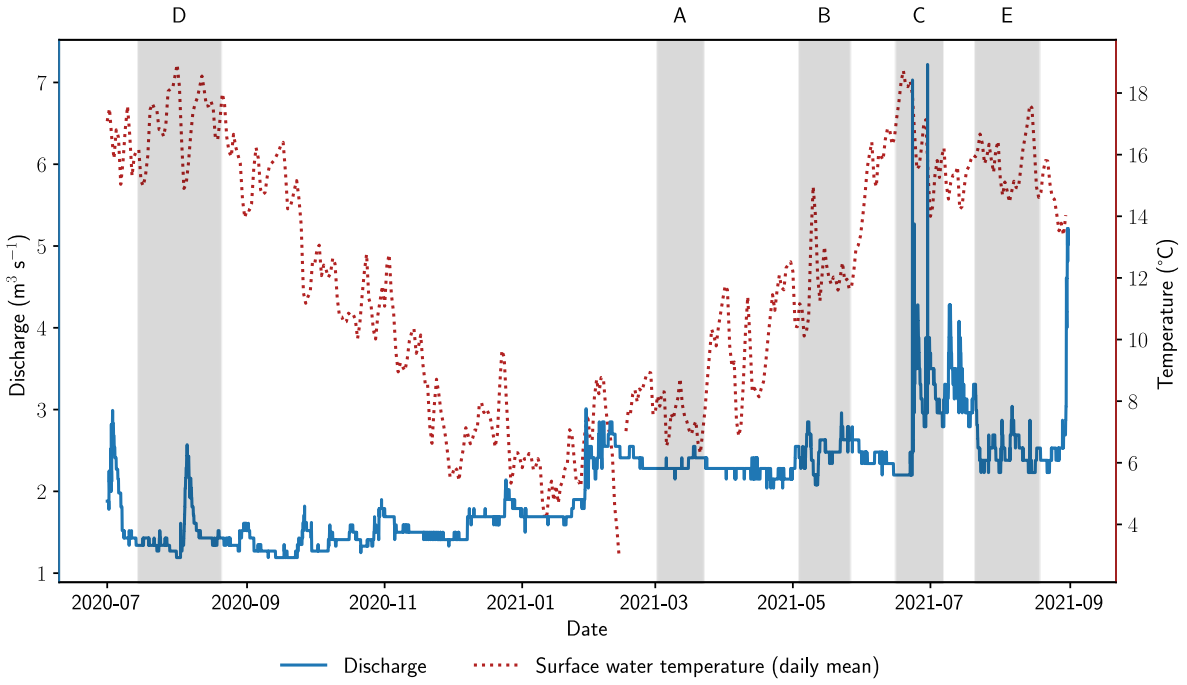

Figure 1: Stream water temperature (daily mean) und discharge. Data was recorded at gauging station Freising Moosach (river chainage: 9.45 km, 4.5 km downstream of the sampling sites), as retrieved from the Bavarian State Office of the Environment.

130

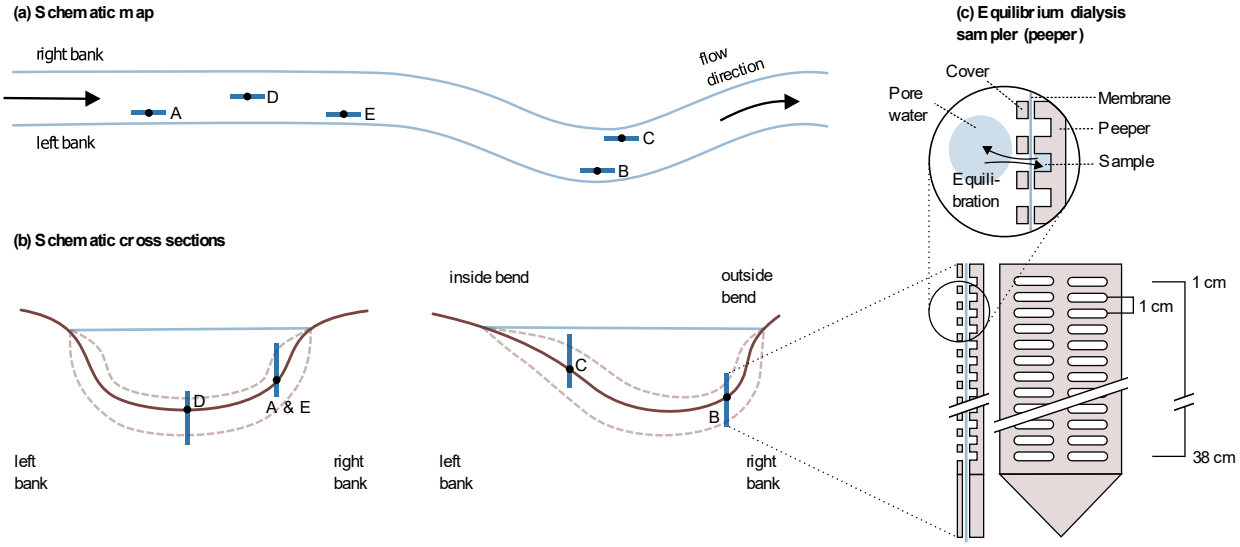

Figure 2: Schematic representation of the five sampling sites along the river (a) and across the river bed (b). In (c), the sampler is schematically drawn, modified after Teasdale et al. (1995) (top: detail, bottom left: side view; bottom right: front view; for clarity, only 12 of the 38 chambers are illustrated).

2.2 Pore-water sampling with a sediment peeper

High-resolution geochemical depth-profiles were obtained at each sampling site with an in-situ equilibrium dialysis sampler (peeper) as described by Hesslein (1976) (see Figure 2c). The body of the peeper was equipped with two rows of 38 chambers in a spatial depth-resolution of 1 cm. All chambers were filled with de-ionized water, covered with a semi-permeable polysulfone membrane with a pore-diameter of 0.2 µm (Pall Corporation, Dreieich, Germany) and fixed with a Plexiglas (PMMA) cover and plastic screws. At each sampling site, the peeper was pushed manually into the stream bed until most chambers were buried in the sediment and only the uppermost chambers had contact with river water. To minimize flow disturbance, peepers were oriented longitudinal to the flow direction as indicated in Fig. 2a.

An equilibrium between the water in the chambers and the surrounding pore-water was obtained by diffusion of dissolved molecules through the membrane during a time period of at least three weeks. This exceeds the recommended equilibration time of minimally two weeks (Teasdale et al., 1995). The extended equilibration time was chosen to allow for recovery of natural geochemical gradients after the disruption caused by placing the peeper. Pore-water samples represent an average of pore water concentrations during the sampling period and diurnal or other short-term temporal fluctuations during this time cannot be detected.

For sampling, the peeper was removed from the sediment and cleaned with de-ionized water. The first column of chambers was used for oxygen measurements and withdrawal of samples for determination of ion concentrations, and the second column was used for CH_4 concentration measurements and analyses of stable carbon isotopes of CH_4. A Clark-type microsensor (Unisense A/S, Aarhus, Denmark) was pierced through the membrane for immediate measurements of dissolved O_2 in the field. The O_2 measurements were conducted on-site within 10 min after removal of the peeper from the sediments to avoid contamination with atmospheric O_2. Liquid samples were then drawn from the same chambers with 5 ml syringes.

10 ml glass vials for CH_4 concentration measurements and stable carbon isotope analysis ($\delta^{13}C$-CH_4) were prepared in the laboratory with 20 µl 10 M NaOH, sealed with rubber butyl stoppers and flushed for at least 2 min with synthetic air (O_2, N_2) to remove background atmospheric CH_4. Immediately before sample injection, a small needle was pushed through the stoppers to allow pressure exchange. Subsequently, with a syringe and needle samples were injected slowly along the side of the vial to avoid degassing. Both needles were removed directly after sample injection. To avoid CH_4 losses to the atmosphere through the membrane, sampling was conducted quickly within 15 min after removal from the sediment. Nevertheless, small amounts of CH_4 could diffuse out through the membrane or escape during sample injection and thus, measured CH_4 concentrations might be slightly underestimated. Samples for ion concentrations were collected in 1.5 ml glass vials and prepared with 10 µl 0.5 M NaOH for anion analysis (Cl^-, NO_3^-, NO_2^-, SO_4^{2-}) or 10 µl 1M HNO_3 for cation analysis (NH_4^+). All samples were withdrawn within 45 min after removal of the peeper. The samples were transported to the laboratory in a cooler and stored refrigerated prior to analysis.

2.3 Chemical and isotopic analyses

Anion and cation measurements

Anion and cation concentrations were determined using ion chromatography, specifically a system of two *Dionex ICS-1100* (Thermo Fisher Scientific, Dreieich, Germany) equipped with *Dionex IonPac™ AS9HC* and *CS12A* columns for anion and cation separation, respectively. Measurements were performed in triplicates and evaluated on the basis of 7 concentration standards (Merck KGaA, Darmstadt, Germany). Concentrations are given as mean values of the triplicates. Analytical uncertainty was <10 % and detection limits were 0.020 mmol L^{-1} for Cl^-, 0.012 mmol L^{-1} for NO_3^-, 0.007 mmol L^{-1} for NO_2^-, 0.008 mmol L^{-1} for SO_4^{2-} and 0.005 mmol L^{-1} for NH_4^+.

CH_4 concentrations and $\delta^{13}C$ measurements of CH_4

Methods for CH_4 sampling and concentration measurements are further developments of standards introduced by the EPA (2001). Sample vials were equilibrated in a water bath at 30 °C for at least 2 h before measurements of headspace CH_4 concentrations with a *Trace 1300* Gas Chromatograph (GC) (Thermo Fisher Scientific, Dreieich, Germany). The GC was equipped with a *TG-5MS* column and flame ionization detector (FID) and calibrated with three standards (Riessner Gase GmbH, Lichtenfels, Germany), Triplicate measurements were performed through manual injection of 250 µl headspace gas. Total CH_4 concentrations in water and gas phase of the sample vials were calculated with Henry's Law according to the equilibrium headspace method first described by Kampbell and Vandegrift (1998).

The same sample vials were used for measuring $^{12}C/^{13}C$ ratios of CH_4 with Cavity Ring-Down Spectroscopy (CRDS), specifically the *G2201-i* Gas Analyzer with a Small Sample Introduction Module (SSIM) (Picarro Inc., Santa Clara, USA) calibrated with two standards (Airgas, Plumsteadville, USA). Reliable results could only be obtained for headspace CH_4 concentrations >30 ppm. This threshold concentration was found in previous experiments (Appendix B). Due to the small available gas volume in the headspace of approximately 7 ml, dilution with synthetic air was necessary and CH_4 concentrations in the analyzer decreased while repeating measurements. Values were only adopted when at least two of three measurements were above the threshold concentration. The standard δ notation is used for representing the results according to Eq. (1) relative to the VPDB standard.

$$\delta[‰] = \left(\frac{R_{Sample}}{R_{Standard}} - 1\right) \cdot 10^3 \quad (1)$$

2.4 Inverse modeling of concentration gradients

The one-dimensional numerical modeling software PROFILE, introduced by Berg et al. (1998), was used to support the interpretation of measured geochemical profiles. The software provides an objective procedure for finding the simplest production-consumption profile which accurately represents the measured concentration gradients. For this, concentration

profiles are divided into different zones with constant production/consumption rates. Then, several best fit results are produced by minimizing the sum of squared deviations (SSD), each representing a different number of these zones. Finally, best fits are compared using statistical F-testing for finding the lowest number of zones which best describe the data.

The model assumes concentration gradients to represent steady state (Berg et al., 1998) which neglects the fact that reaction rates in the HZ show temporal variability (Marzadri et al., 2012). However, the pore-water samples obtained with the sediment peeper represent a time-averaged state during the total sampling period of at least 3 weeks. The relative contribution of short-term fluctuations decreases with the length of the averaged time. Therefore, as a first approximation we assume that after 3 weeks this dynamic component is small particularly in the deeper HZ and can be neglected.

Boundary conditions (BCs) were set as follows: for O_2, NO_3^- and SO_4^{2-} a fixed concentration was set the top and a zero flux BC at the bottom of the profile; for CH_4 a fixed concentration and zero flux BC were set at the top of the profile, similar to what was used by Norði and Thamdrup (2014). Positive production rates were only allowed for SO_4^{2-} and CH_4 while for O_2 and NO_3^- only negative rates (consumption) were permitted. Biotubation and irrigation were neglected. Molecular diffusion coefficients in water D^0 ($m^2\ s^{-1}$) were calculated based on Boudreau (1997) as a function of the average water temperature during the equilibration period. Sediment diffusion coefficients D_s were determined as a function of D^0 based on an empirical relation (Iversen and Jørgensen, 1993). More details and calculated diffusion coefficients D^0 and D_S are given in Appendix C.

2.5 DNA extraction, qPCR and 16S rRNA gene sequencing

At location C, an additional sediment core was taken for depth-resolved microbiological analyses via DNA extraction, quantitative PCR and 16S rRNA gene sequencing. For this, a coring tube with an inner diameter of 42 cm was cut open lengthwise, cleaned with ethanol and distilled water and closed again with tape. The core was taken by manually pushing the tube into the sediment right next to the peeper, pulling it out and transferring it to the laboratory. There, the tape was removed for opening the tube and allowing access to the sediment core. The sediment was split into 10 subsamples with a resolution of 2 cm in the upper 12 cm depth and 3 cm below. All samples were immediately frozen and stored at -22 °C until further analysis. For each sampled depth, we performed four biological replicates of DNA extraction. Total DNA was extracted from 0.5 g of sediment as previously described (Vuillemin et al., 2019). DNA templates were diluted 1:100 in ultrapure PCR water (Roche, Germany) and used in qPCR amplifications with updated 16S rRNA gene primer pair 515F (5′- GTG YCA GCM GCC GCG GTA A -3′) and 806R (5′- GGA CTA CNV GGG TWT CTA AT -3′) to increase our coverage of archaea and marine clades and run as previously described (Pichler et al., 2018). All qPCR reactions were set up in 20 µL volumes with 4 µL of DNA template, 20 µL SsoAdvanced SYBR Green Supermix (BioRad, Feldkirchen, Germany), 4.8 µL Nuclease-free H_2O (Roche, Germany), 0.4 µL primers (10 µM; biomers.net) and 0.4 µL $MgCl_2$ and carried out on a CFX-Connect qPCR machine for gene quantification. For 16S rRNA genes, we ran 40 PCR cycles of two steps corresponding to denaturation at 95 °C for 15 s, annealing and extension at 55 °C for 30 s. All qPCR reactions were set up in 20 µL volumes with 4 µL of DNA template and performed as previously described (Coskun et al., 2019). Gel purified amplicons of the 16S rRNA genes were quantified in triplicate using QuantiT dsDNA reagent (Life Technologies, Carlsbad, USA) and used as a standard. An EpMotion 5070

automated liquid handler (Eppendorf, Hamburg, Germany) was used to set up all qPCR reactions and to prepare the standard curve dilution series spanning from 10^7 to 10^1 gene copies. Reaction efficiency values in all qPCR assays were between 90 % and 110 % with R^2 values >0.95 for the standards.

For 16S rRNA gene library preparation, qPCR runs were performed with barcoded primer pair 515F and 806R as described previously (Pichler et al., 2018). In brief, 16S rRNA gene amplicons were purified from 1.5 % agarose gels using the QIAquick Gel Extraction Kit (Qiagen, Hilden, Germany), quantified with the Qubit dsDNA HS Assay Kit (Thermo Fisher Scientific, Dreieich, Germany), normalized to 1 nM solutions and pooled. Library preparation was carried out according to the MiniSeq System Denature and Dilute Libraries Guide (Illumina, San Diego, USA). Sequencing was performed on the Illumina MiniSeq platform at the Geo-Bio LMU Center. We used USEARCH version 10.0.240 for MiniSeq read trimming and assembly, OTU picking and 97 % sequence identity clustering (Edgar, 2013), which, as we showed previously, captures an accurate diversity represented within mock communities sequenced on the same platform (Pichler et al., 2018). OTU representative sequences were identified by BLASTn searches against SILVA database version 132 (Quast et al., 2012). To identify contaminants, 16S rRNA genes from extraction blanks and dust samples from the lab were also sequenced in triplicate (Pichler et al., 2018). These 16S rRNA gene sequences were used to identify any contaminating bacteria (e.g. *Acinetobater*, *Bacillus*, *Staphylococcus*) and selectively curate the OTU table.

3 Results and discussion

3.1 Concentration profiles show steep geochemical gradients and the formation of a complex redox zonation

The geochemical profiles obtained in the HZ of river Moosach are shown in Figure 3. The total depth of the profiles depended on how deep the peeper was pushed into the ground and varied between 27 cm and 38 cm. Above the sediment-water interface, in-stream concentrations were 270-300 µmol L^{-1} for dissolved O_2, 280-380 µmol L^{-1} for NO_3^-, 240-360 µmol L^{-1} for SO_4^{2-} and 1270-1650 µmol L^{-1} for Cl^-. Surface water concentrations as measured on the day of sampling are displayed as vertical beams above the sediment-water interface in Fig. 3.

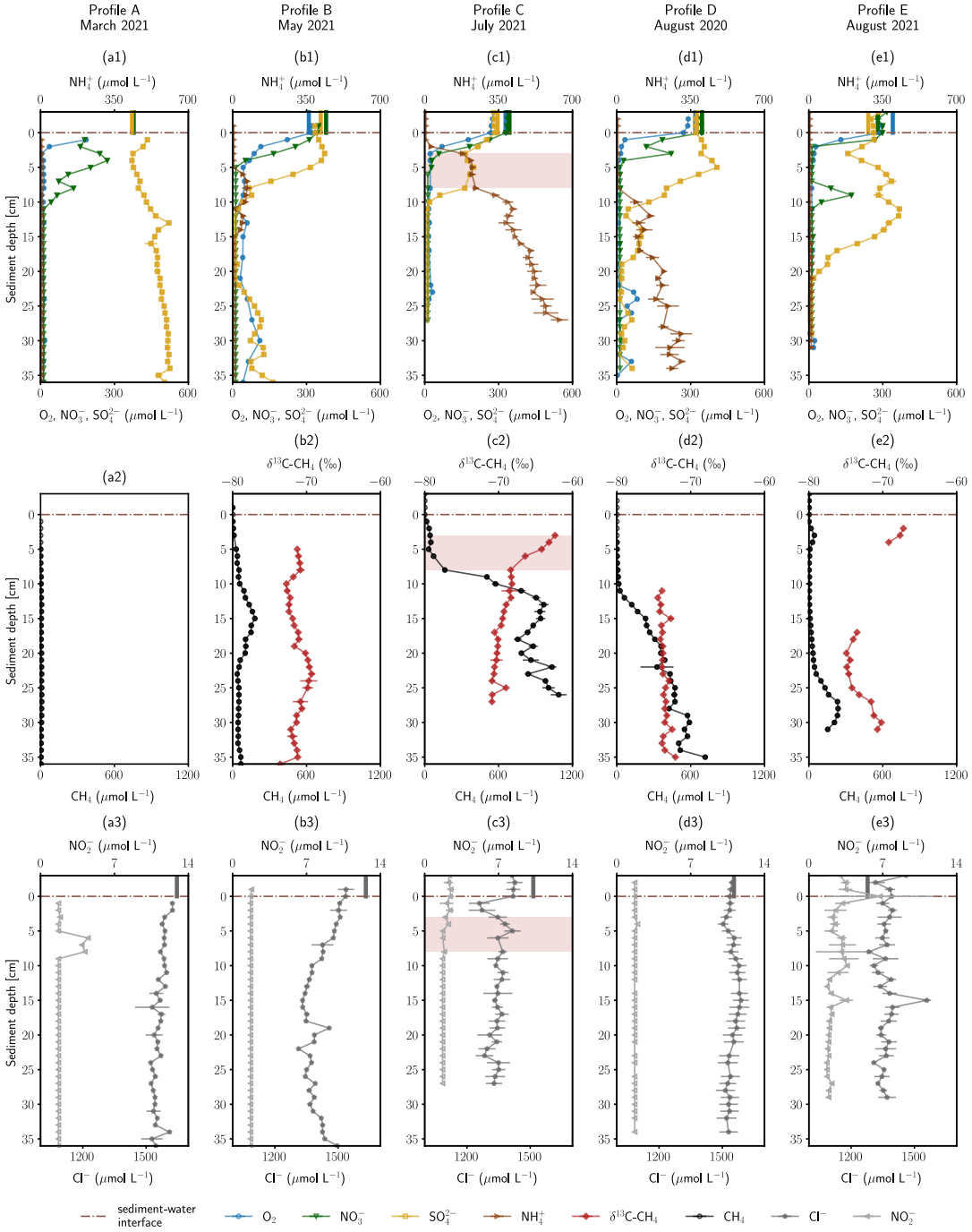

Figure 3: Depth-resolved profiles of hyporheic pore-water geochemistry at five sampling sites. Panels (a1) to (e1) show O_2, NO_3^-, NH_4^+ and SO_4^{2-} concentrations, panels (a2) to (e2) CH_4 concentrations and $\delta^{13}C\text{-}CH_4$ values and panels (a3) to (e3) NO_2^- and Cl^- concentrations. Empty markers indicate values outside the range of used standards. Error bars show standard deviations of independent measurements (n=3). Vertical lines above the sediment-water interface are concentrations measured in the surface water at the sampling date. Red background color highlights an enrichment in $\delta^{13}C\text{-}CH_4$. Profiles are ordered by season.

Land-use in the catchment is predominantly agriculture and leaching of fertilizers presumably adds NO_3^- to river and groundwater, but values stayed clearly below the threshold of the EU Nitrates Directive of 50 mg L^{-1} (806 µmol L^{-1}). SO_4^{2-} concentrations in the surface water were strikingly high for a freshwater river, especially in spring. Groundwater in the quarternary aquifer, the groundwater body hydraulically connected to the river, showed SO_4^{2-} concentrations between 448 and 573 µmol L^{-1} during 2007-2020 as measured in an observation well approximately 1.6 km south-west of the sampling sites (Bavarian State Office of the Environment). Peat can contain substantial amounts of carbon-bonded sulfur and pyritic sulfides (Spratt Jr et al., 1987; Casagrande et al., 1977) and SO_4^{2-} can be released due to pyrite and organic matter oxidation (Vermaat et al., 2016), likely so in the drained moor areas in the foothills of the Munich Gravel Plain that the Moosach river crosses. In an agricultural watershed sulfur fertilizers can also be a source of elevated SO_4^{2-} concentrations in shallow aquifers (Spoelstra et al., 2021).

Below the sediment-water interface dissolved O_2 concentrations decreased within few centimeters in all sampled profiles and remained at <10 µmol L^{-1} deeper down with only few exceptions. Steep O_2 gradients and anoxic conditions just below this narrow aerobic zone were to be expected, because the river Moosach is strongly altered by human engineering including controlled discharge conditions, a very low gradient, slow flow velocities and deposits of fine, organic-rich materials. In profile B, O_2 concentrations were higher compared to all other sites (20-80 µmol L^{-1} below 3 cm depth). This may be due to higher surface water influxes in the coarser gravelly sediment as opposed to the fine deposits found at the other sites. However, even between 10-20 cm depth, where CH_4 concentrations peaked in a sedimentary layer dominated by silt, O_2 was present at concentrations between 20 and 60 µmol L^{-1}. These high O_2 concentrations appear to be rather implausible in this zone where CH_4 is produced through methanogenesis, a strictly anaerobic process. An explanation could, however, be contamination with atmospheric O_2 during field measurements. Similarly, profile D shows anomalies in the O_2 data with concentration peaks at 23-26 cm, 30 cm and 33 cm depth. These may also be attributed to measurement artefacts since they are located deep in the methanogenic zone where strictly anoxic conditions generally prevail.

Similar to dissolved O_2, NO_3^- concentrations decreased from 280-380 µmol L^{-1} in river water to concentrations of <12 µmol L^{-1} (detection limit) within a few centimeters. In contrast, the conservative tracer Cl^- did not disappear in a comparable manner which may demonstrate that microbial consumption and not dilution or mixing was responsible for the development of these steep chemical gradients. A peak of NO_2^- in profile A exactly where the NO_3^- gradient is located (6-8 cm) indicates bacterial NO_3^- reduction to NO_2^-, possibly as an intermediate in denitrification (Fig. 2c). In profiles B-E O_2 reduction and denitrification zones were very close and both gradients overlapped. Oxygen reduction and denitrification zones seem to be only millimeters wide, similar to what was described for other freshwater sediments in the literature (Raghoebarsing et al., 2006). In profile D a peak between 8-10 cm depth with a maximum of 173 µmol L^{-1} stands out that coincides with a reduction of SO_4^{2-} concentrations.

SO_4^{2-} concentration profiles showed some distinctive features. In profiles A and B, concentrations slightly increased towards the bottom of the profile. This could be connected to the intrusion of upwelling, reduced groundwater with a higher SO_4^{2-} concentration compared to surface water. Rising Cl^- concentrations in the lower third of profile B support this interpretation, since they reach 1491 µmol L^{-1}, a value very similar to groundwater Cl^- concentrations of 1440-1495 µmol L^{-1} in recent years (2016-2020) (Bavarian State Office of the Environment). Further, in profiles B and D, SO_4^{2-} concentrations increased in the upper parts of the profiles in 0-3 cm and 0-5 cm depth, respectively, and also in profile E between 3-7 cm and 9-11 cm depth. Here, a biogeochemical source, for example re-oxidation of H_2S travelling upwards from more reduced zones, could explain the observed trends. Below, in 3-11 cm (profile B), 5-11 cm (profile C) and 12-22 cm depth (profile E) concentrations declined, potentially through bacterial SO_4^{2-} reduction. This interpretation is supported by a sulfidic smell during sampling. Interestingly, in profile C SO_4^{2-} concentrations decreased significantly not only between 8-11 cm, but also between 0-3 cm depth, concurrently with decreases in O_2 and NO_3^- concentrations. One possible interpretation is a dilution effect at the clogged sediment surface, as also suggested by simultaneous decreases in Cl^- (Fig. 3 (c3)) and Ca^{2+} (data not shown) concentrations. But the data could also show the co-occurrence of oxic and anoxic micro-niches in close proximity, a situation that has also been described previously (Storey et al., 1999; Triska et al., 1993).

NH_4^+ concentrations in most profiles (C-E) consistently increased with sediment depth. While maximal concentrations in profiles C and D were 116 µmol L^{-1} and 308 µmol L^{-1}, respectively, in profile C values reached a level of >1000 µmol L^{-1}. During biodegradation of organic matter, NH_4^+ is released when nitrogenous compounds are transformed through ammonification (Ladd and Jackson, 1982). Increases with depth show progressive decomposition and high NH_4^+ concentrations can be seen as a proxy for a high content of microbially degraded organic matter in the sediment. Thus, organic carbon content seems to be significantly lower in location E compared to C and D. In location A, NH_4^+ concentrations even stayed below the detection limit (<5 µmol L^{-1}). Profile B has elevated NH_4^+ concentrations in 6-14 cm depth and values below the detection limit elsewhere.

Similar to NH_4^+ concentrations, CH_4 concentrations generally increased with depth and were highest in profile C, followed by profile D. In profile A, where NH_4^+ concentrations were lowest compared to all other profiles, CH_4 concentrations stayed below 10 µmol L^{-1}. More complex were the observed CH_4 gradients in profiles B and D. In profile B, CH_4 peaked at a concentration of 180 µmol L^{-1} in a sediment depth of 15 cm. Below, from 23 cm onwards, concentrations decreased and stayed around 50 µmol L^{-1}. CH_4 concentrations of profile E revealed a small peak (44 µmol L^{-1}) at 3 cm depth, showed very low concentrations of <10 µmol L^{-1} between 5-15 cm and rose again up to 237 µmol L^{-1} at a depth of 28 cm.

Generally, a tendency of increasing CH_4 concentrations with higher surface water temperatures can be observed. Profiles A and B, measured in spring, showed significantly lower CH_4 concentrations than those sampled in summer. However, comparing profiles C, D and E, all measured in summer, substantial differences in total CH_4 concentrations are eye catching. By far the highest CH_4 concentrations were measured in July 2021 (T_M = 16.6 °C for profile C, Tab. A1) although surface water temperatures were slightly lower than in August 2020 (T_M = 17.1 °C for profile D). CH_4 concentrations in profiles C, D

and E exceeded the CH_4 saturation concentrations of 170 µmol L^{-1}, 282 µmol L^{-1} and 202 µmol L^{-1}, respectively (calculated using PhreeqC (Parkhurst & Appelo, 2013) and for the mean surface water temperature during the sampling period, a water depth of 0.6 m, 1.2 m and 0.7 m, respectively, and for a sediment depth of 30 cm). These concentrations are expected to cause the formation of gas bubbles. In profile C, a CH_4 concentration of 19800 µmol L^{-1} measured in 27 cm depth (not displayed in Fig. 3 since it is far out of the axes' range) implies direct contact with a gas bubble. In comparison, profile E, measured in August 2021, exhibits low concentrations despite the summer temperatures (T_M = 15.8 °C). Varying organic matter contents at the three sites might explain these differences and seems to be a determining parameter for total CH_4 production, as inferred from differences in NH_4^+ concentrations. When complex organic molecules are degraded by microbes, not only NH_4^+ is released, but also educts for methanogenesis like H_2, CO_2, acetate and methylated compounds like methanol (Capone and Kiene, 1988). The degradation of organic carbon is therefore a driver of methanogenesis and we see a correlation between CH_4 and NH_4^+ concentrations (see Fig. D1). This finding is also consistent with previous reports from stream sediment incubations (Bodmer et al., 2020; Romeijn et al., 2019; Bednařík et al., 2019; Crawford et al., 2017).

Cl^- can be viewed as a conservative tracer. As mentioned above, one irregularity is a sudden concentration decrease in the first centimeters of profile C. This could show the effect of clogging, because fine deposits fill the pore space and reduce hyporheic exchange. Interesting is also that Cl^- concentrations decrease in the middle section of profile B. Cl^- concentrations in profiles A, D and E do not exhibit any trends, fluctuations are highest in profile E.

3.2 Explaining redox zones with sediment heterogeneities and hyporheic exchange fluxes

Observed concentration profiles at the different stream sites showed distinct characteristics and were very heterogeneous. The divergence of the profiles becomes particularly clear when comparing profiles A and E that show hardly any similarities although they were sampled at two very similar sites. In March, where river water is well oxygenated with average surface water temperatures of 7.5 °C (profile A), SO_4^{2-} concentrations were high (>300 µmol L^{-1}) throughout the profile and almost no CH_4 was produced. In August (profile E), clear gradients in SO_4^{2-} and CH_4 concentrations together with nearly constant Cl^- concentrations point towards a high activity of SRB and methanogens. As mentioned earlier, higher stream water temperatures in summer (profile E) could be the reason for higher microbial activity compared to early spring (profile A). However, the influence of temperature on GHG emissions from rivers has been discussed controversially. Increasing GHG production with rising temperatures was observed in laboratory incubations of river sediments (Comer-Warner et al., 2018; Shelley et al., 2015) while Silvennoinen et al. (2008) found that 55 % of all CH_4 emissions from the Temmesjoki River were released during winter time.

In our data, temperature alone may not explain the differences between the two profiles A and E. Concentration gradients in profile E do not follow the generally known redox zonation (Canfield and Thamdrup, 2009). The assumption that stream water enters the HZ at the stream-water interface and that electron acceptors are consumed successively can neither explain the complex SO_4^{2-} dynamics, nor the deep NO_3^- peak. A possible reason could be surface water entering the sediment bank from the side, maybe in a sandier layer, such that sample depths represent different and varying flow path lengths of hyporheic

fluxes. This is further illustrated in Fig. 4e. Stream water entering the bank from the side could be an additional reason (besides cold temperatures and potentially low organic matter degradation) for low CH_4 levels in profile A (Fig. 4a). Figure 4 schematically shows the hypothesized sedimentary characteristics and potential hyporheic fluxes at all five sampling sites.

Sediment stratification and resulting hyporheic fluxes can also help in understanding profile B. In the top section, as it would be expected, O_2, NO_3^- and SO_4^{2-} are consumed consecutively and CH_4 concentrations rise, but below 15 cm depth, we see the reverse trends. A lens of fine material in an otherwise gravelly sediment would be a plausible explanation for this observation (Fig. 4b). In fact, very fine sediment was found below 11 cm depth and gravel above, but the sediment core did not cover the lowest part of the profile (Appendix A). Hyporheic flow velocities outside the fine lens would be faster than inside and thus, although path lengths at the bottom are longer, contact times have been shorter than in the central part of the profile. This would mean that we see the methanogenic zone in the central part and the sulfate reduction zone at the bottom of profile B, depending on the available time for reactions along the flow path.

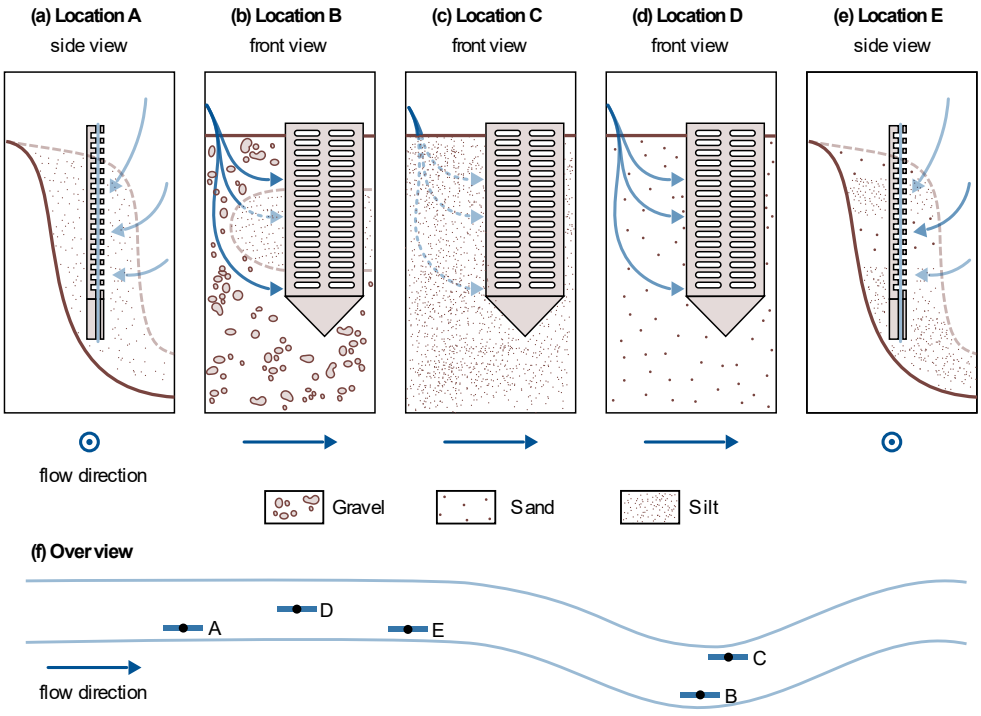

Figure 4: Schematic representation of potential hyporheic flow paths (blue arrows) at the five sampling sites. For locations A and E, a side view was chosen and for locations B, C and D a front view. Where the front view is shown, flow direction in the river is from left to right and where the side view is shown flow direction is out of the drawing plane. The color strength of the arrows corresponds to the expected magnitude of hyporheic fluxes. The sediment composition is schematically indicated. Quantitative data on the sediment composition at the five locations can be found in Appendix A.

Also profile C deviated from the commonly assumed redox zonation. Bacterial SO_4^{2-} reduction appeared to occur concurrently with O_2 reduction and denitrification, possibly in co-occurring oxic and anoxic zones (Storey et al., 1999). Alternatively, this may be caused by dilution effects in the upper centimeters of the profile. Also unexpected were stagnating SO_4^{2-} concentrations with a slightly convex concentration gradient between 3-8 cm depth. There might be an additional SO_4^{2-} source, maybe recycling of reduced sulfur species from deeper zones or some cryptic sulfur cycling as has been suggested in the context of S-DAMO in freshwater environments (Ng et al., 2020; Norði et al., 2013). But also here, heterogeneous flow paths, for example due to wood and plant parts, could affect measured profiles such that water travel times do not linearly increase with depth.

The profile most clearly following the thermodynamic sequence was profile D. Here, O_2 was consumed first, followed by NO_3^- and bacterial SO_4^{2-} reduction. Only after all other electron acceptors were consumed, CH_4 concentrations began to rise with depth.

When discussing the influence of hyporheic fluxes on redox zonation, it needs to be noted that not only spatial heterogeneities, but also temporal dynamics may play a key role. For example, extreme events can alter the chemistry of infiltrating surface water, as well as hyporheic flow path lengths and residence times, thus impacting hyporheic geochemistry in multiple ways (Zimmer & Lautz, 2014). In this study in particular, location C might have been impacted by two high flow events during the sampling period. Further, seasonal changes in river-groundwater mixing can potentially impact redox conditions and microbial populations (Danczak et al., 2016). However, fine sediments have been shown to reduce hyporheic exchange (Sunjidmaa et al., 2022). The combination of very fine deposits and stable, controlled hydrologic conditions is expected to limit hyporheic exchange and may also temper temporal dynamics in the HZ of river Moosach.

3.3 Stable carbon isotopes of CH_4 reveal the importance of hydrogenotrophic methanogenesis and the roles of diffusive versus biotic processes in reducing CH_4 concentrations beneath the sediment surface

Figure 3 also shows $\delta^{13}C$-CH_4 values for Profiles B - E in panels (a2) to (e2). CH_4 concentrations at location A were too low for isotopic analyses. In profile B, $\delta^{13}C$-CH_4 values were on average -74 ‰. $\delta^{13}C$-CH_4 values were very similar, but slightly shifted in a range of <3 ‰ with an increasing trend (top to bottom) between 5-8 cm and 10-23 cm depth and a decreasing trend between 8-12 cm and 23-31 cm depth. These variations were too small to be taken as an indication for any microbially mediated processes and could be explained by diffusion controlled isotope fractionation.

In profile C on the other hand, two sections are clearly evident (see Fig. 3 (c2)). From bottom to top, between 27 cm and 8 cm depth, $\delta^{13}C$-CH_4 values increased almost linearly from -71 ‰ to -69 ‰, then the slope changed abruptly and an isotopic enrichment from -69 ‰ to -62 ‰ can be seen between a sediment depth of 8 cm and 3 cm. Isotopically lighter $^{12}CH_4$ is transported and consumed faster than heavier $^{13}CH_4$ which leads to an isotopic enrichment of the remaining CH_4 pool in the heavier $^{13}CH_4$ (Whiticar et al., 1986). This isotopic shift towards heavier isotopes from 8 cm to 3 cm combined with decreasing CH_4 concentrations, therefore, clearly indicates microbial CH_4 consumption. Interestingly, the measured O_2 gradient lied above this zone (0-3 cm depth), while denitrification potentially occurred in exactly this depth (0-5 cm) and SO_4^{2-} concentrations stagnated around 176 µmol L^{-1} in 3-8 cm depth. Inverse modeling and the microbial community distribution at location C may

help interpreting the details of CH_4 oxidation as outlined in detail below (Sec. 3.4 and 3.5). The zone of $^{13}CH_4$ enrichment in profile C, where CH_4 oxidation is inferred, is highlighted by a red background color in Fig. 3 & 5 to visually help differentiating this zone from the rest of the profile. The slight isotopic enrichment of $\delta^{13}C$-CH_4 of a few per mil below, between 27 cm und 8 cm depth, is likely affected by diffusion-controlled stable isotope fractionation. It is striking that CH_4 concentrations steeply decrease already between 12 cm and 8 cm depth, beneath the zone of strong $^{13}CH_4$ enrichment. Apparently, microbial consumption only impacts the upper part of the gradient, while diffusive transport shapes the lower part of the gradient.

In profile D, $\delta^{13}C$-CH_4 values were on average -71 ‰ and the isotopic composition stayed nearly constant. At least above 10 cm depth, where CH_4 concentrations were high enough for repeated isotope measurements, results suggest that microbial CH_4 oxidation did not play a key role in removing CH_4 from the HZ at location D. In profile E, reliable $\delta^{13}C$-CH_4 values could only be obtained in 2-4 cm and 17-21 cm depth. In the upper zone, values lay between -67 ‰ and -69 ‰, in the lower between -71 ‰ and -75 ‰ with a tendency towards less negative values in the lowest part of the profile. Since differences between isotope values at the top and the bottom were within a few per mil and there is a large data gap between 5-16 cm, data interpretations are difficult. The slightly heavier carbon isotopes of CH_4 at the top of the profile may be an indication for aerobic or anaerobic oxidation, but there is no additional evidence for this interpretation.

A kinetic isotope effect also occurs during CH_4 production and is larger for hydrogenotrophic than for acetoclastic methanogenesis (Krzycki et al., 1987). Here, $\delta^{13}C$-CH_4 values in the methanogenic zone were consistently lower than -60 ‰ which is characteristic for hydrogenotrophic methanogenesis (Whiticar, 1999). This fits well to findings of Bednařík et al. (2019) and Mach et al. (2015) who found that hydrogenotrophic methanogenesis was the dominant CH_4 production pathway in the HZ of the Elbe and Sitka rivers.

At all sampling sites CH_4 concentrations decreased towards the sediment surface, but in most of the profiles, where $\delta^{13}C$-CH_4 data was available, this was not accompanied by a significant enrichment in the heavier $^{13}CH_4$. Diffusive processes in these cases appear to be responsible for reducing CH_4 concentrations between the methanogenic zone and the upper part of the riverbed. At the sediment-water interface only very low CH_4 concentrations were found in all profiles (A-E), pointing towards small diffusive fluxes across the sediment-water interface. This finding is surprising, because we expected high CH_4 concentrations and large fluxes to the water column and towards the atmosphere. However, it must be noted that we looked at diffusive CH_4 fluxes within the HZ and did not cover the possible generation and transport of gas bubbles. The contribution of these bubbles to total CH_4 fluxes across the sediment-water interface at river Moosach remains unknown, but ebullition might be a significant contributor to CH_4 effluxes as suggested in the literature (DelSontro et al., 2010; McGinnis et al., 2016). As explained above, isotopic evidence indicated a significant contribution of microbial CH_4 consumption to a reduction of diffusive CH_4 fluxes only in profile C. In all other profiles, it is possible that CH_4 is either oxidized at rates too low to alter its isotopic composition or that CH_4 oxidation takes place close to the sediment-water interface were CH_4 concentrations were too low for the isotope measurements. In both cases, this implies a limited relevance for the reduction of diffusive CH_4 fluxes. To gain further insights into aerobic and anaerobic CH_4 oxidation, the modeling software PROFILE was applied (Sec. 3.4).

One reason for the observed methane oxidation processes in location C could be an increased supply of O_2 and NO_3^- during the two high-flow events in the sampling period.

3.4 Inverse modeling of concentration gradients as a basis for discussing aerobic versus anaerobic oxidation of CH4

Figure 5 shows the results of inverse concentration gradient modeling with the software tool PROFILE. Overall, the modeled and measured concentrations agreed well to each other, especially for CH_4 and SO_4^{2-}. In the more complex CH_4 and SO_4^{2-} profiles, often several consumption zones were detected. Deviations of modeled from measured data were more pronounced for O_2 gradients in profiles B and D, as well as for the NO_3^- gradient in profile E. Here, the model could not capture the data well, potentially because higher concentration values and outliers in deeper sediment depths might have biased the fit in the upper gradient, resulting in broader oxygen reduction- and denitrification zones.

In the PROFILE software, vertical transport can be attributed to diffusion, bioturbation, and irrigation. However, exchange flows control river bed biogeochemistry and solute transport in the HZ (Bardini et al., 2012; 2013). As a result, the disregard of advective solute transport with hyporheic exchange flows may lead to an underestimation of O_2, NO_3^- and SO_4^{2-} reduction rates since entering surface water increases the availability of educts for geochemical reactions. Where pore water movement is slow, O_2 uptake is proportional to the rate of solute influx (Rutherford et al., 1993; 1995). On the other hand, CH_4-rich pore water is diluted with stream water and modeled CH_4 oxidation rates may, therefore, rather be over-estimated. Yet, hydraulic conductivities as calculated using the empirical formula of Beyer (1964) are relatively low ($<8 \cdot 10^{-5}$ m s^{-1}) in the fine-grained deposits of the Moosach river (Table A4) which reduces the influence of the advective component in locations A, C and E. The model is applied to find the depths of reactive production and consumption zones. Calculated reaction rates are used to compare profiles, but due to the limitations described above, absolute values should not be over-interpreted.

Depth-integrated modeled O_2 consumption rates were in the range 0.10-0.41 mmol m^{-2} d^{-1}. NO_3^- reduction rates were found to be between 0.18 and 0.29 mmol m^{-2} d^{-1} in profiles C, D and E while only 0.08 mmol m^{-2} d^{-1} of NO_3^- were consumed in profile B in a much narrower DZ. Using PROFILE for the interpretation of concentration gradients in a microcosm study, Norði and Thamdrup (2014) found rates of 11.4 mmol m^2 d^{-1} for O_2 and 0.9 mmol m^2 d^{-1} for NO_3^- uptake which is about 30-100 times higher for O_2 and 3-12 times higher for NO_3^- than simulated here. In their work both O_2 and NO_3^- were consumed completely within millimeters building much steeper gradients than observed in this study. Modeled ORZs in profiles C and E were 4.5 cm and 3.5 cm wide, in profiles B and D even 7 cm, in the latter two cases partly due to poor fits. Additionally, as mentioned above, an underestimation of modeled O_2 and NO_3^- uptake rates is likely since the model does not include advective hyporheic exchange fluxes. In profile C, stream water can easily enter the sandy stream bed and flow velocities are expected to be higher than close to the banks, O_2 uptake and denitrification are supposed to be much larger than suggested by the diffusive model.

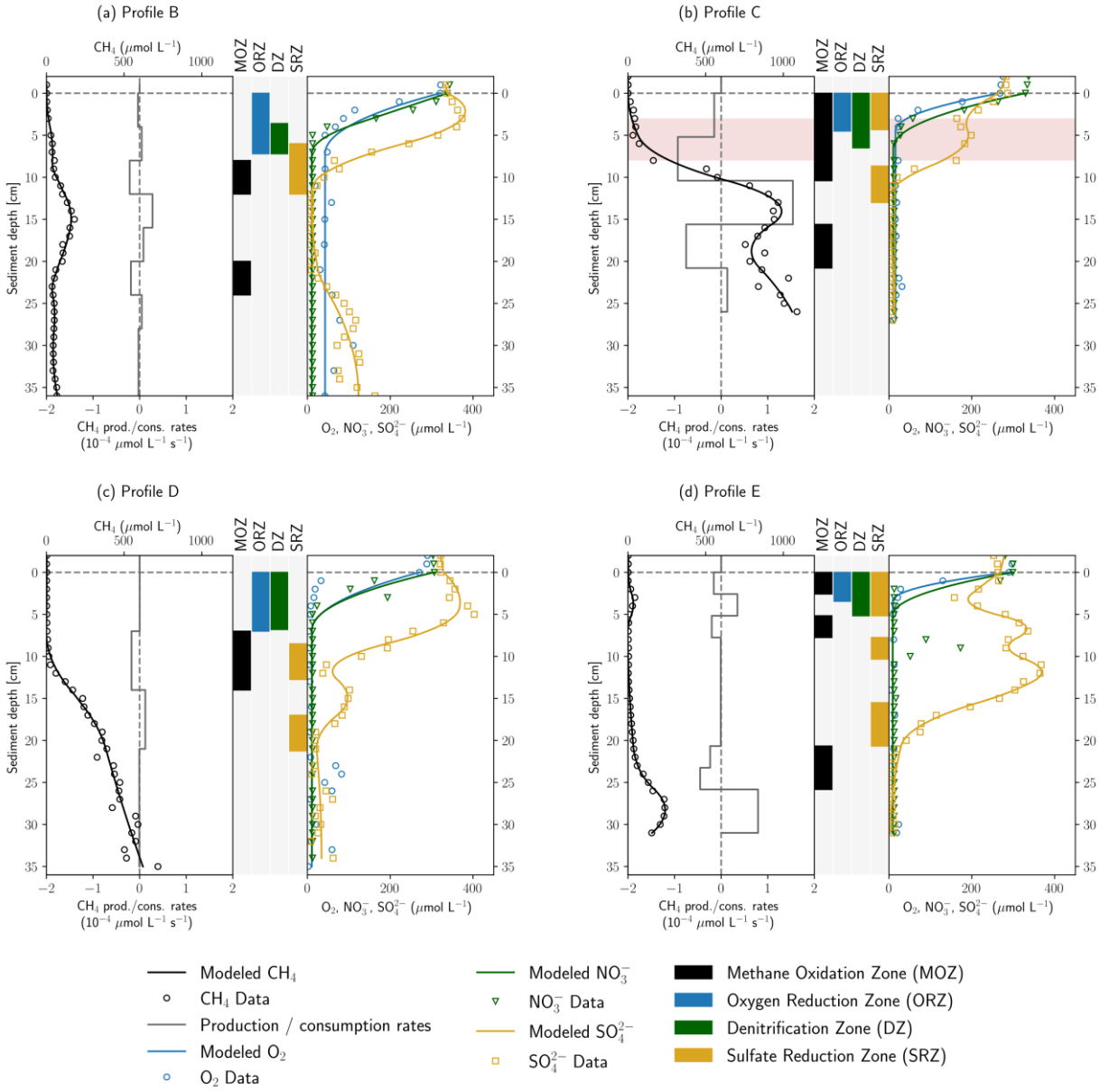

Figure 5: Results of concentration gradient modeling using the PROFILE software for profiles B-E. In each panel (a)-(d), the left side shows modeled and measured CH_4 concentrations as well as modeled CH_4 production and consumption rates. In the center, the depth ranges of MOZ, ORZ, DZ and SRZ are highlighted. Zones with very low consumption rates ($<5 \cdot 10^{-6}$ µmol L^{-1} s^{-1}) were not identified. On the right, measured and modeled O_2, NO_3^- and SO_4^{2-} concentrations are shown. Rates are not displayed for electron acceptors for reasons of clarity. Red background color in panel (b) highlights an enrichment in $\delta^{13}C$-CH_4.

In profile B a single SRZ was found in 6-12 cm depth whereas SO_4^{2-} reduction takes place in several depth ranges in profiles C-E. Total modeled SO_4^{2-} consumption ranged from 0.06 mmol m^{-2} d^{-1} (profile D) to 0.43 mmol m^{-2} d^{-1} (profile E). This is in line with modeling results of Norði et al. (2013) who found 0.2 mmol m^{-2} d^{-1} sulfate reduction in a freshwater lake sediment. Yet, directly measured rates were 10 times higher in their study showing a discrepancy between modeled and measured values. Jørgensen et al. (2001) found SO_4^{2-} reduction rates of 0.65-1.43 mmol m^{-2} d^{-1} in the black sea using the same model. In profiles B and D SRZs were located beneath ORZ and DZ as it would be expected, but in profiles C and E the uppermost SRZ overlapped with ORZ and DZ. For profile C, the concurrent decrease of O_2, NO_3^- and SO_4^{2-} has already been discussed in Sec. 3.1 (anaerobic micro-niches or dilution effects at a clogged sediment surface). For profile E, NO_3^- is completely consumed between 1-2 cm depth in a very narrow DZ and SO_4^{2-} concentrations start to decrease from 1 cm onwards, most likely right after NO_3^- has been removed from the system. The model did not capture these very steep gradients precisely, because data resolution was too coarse. Likewise, the sudden NO_3^- peak in 9 cm depth in profile E was not recognized, because too few data points in the peak were available.

MOZs were found in every profile even where $\delta^{13}C\text{-}CH_4$ values were stable, but rates were generally low ($<2\cdot10^{-4}$ µmol L^{-1} s^{-1}). For example, in profiles B and E, CH_4 was modeled to be consumed on both sides of the peaks in 3 cm and 15 cm depth, at rates of 0.06-0.07 mmol m^{-2} d^{-1} and 0.04-0.05 mmol m^{-2} d^{-1}, respectively. It is not surprising that these small consumption rates did not change the isotopic composition of CH_4. A single MOZ was found in profile D in 7-14 cm depth with a depth-integrated rate of 0.11 mmol m^{-2} d^{-1}. In profile C, 0.42 mmol CH_4 m^{-2} d^{-1} were simulated to be oxidized between 0-10.4 cm depth, but with a 6 times higher rate below the ORZ (5.2-10.4 cm). This upper MOZ falls together with the observed enrichment in $\delta^{13}C\text{-}CH_4$ between 3-8 cm depth.

The model was applied to help identifying the electron acceptors responsible for CH_4 oxidation. This involves checking for overlaps between MOZ and ORZ, DZ and SRZ. In profiles A and D, the MOZ only overlaps the SRZ combined with very low modeled oxidation rates. Profiles C and E show overlaps of all zones in the uppermost centimeters where $\delta^{13}C\text{-}CH_4$ measurements were not available due to low CH_4 concentrations. Here, aerobic methane oxidation could potentially take place. In profile C, the modeled oxidation rate increased significantly below the ORZ and intersected with the DZ in the upper and the SRZ in the lowest part. This could point towards AOM coupled to denitrification or bacterial sulfate reduction in anoxic micro-niches, but since gradients were very steep and trace oxygen might also have been present, the delineation of the relevant electron acceptor is not possible. The higher CH_4 oxidation rate in the presence of NO_3^- compared to O_2 in profile C, if valid, may show a situation in the HZ of the Moosach river similar to sediments of lake Constance. Measurements of Deutzmann et al. (2014) showed that N-DAMO was the major CH_4 sink although the community of aerobic methanotrophs would have been capable of oxidizing the entire methane flux. Limiting for aerobic oxidation was the available CH_4 after passing through the denitrification zone where most of it was already oxidized. Nonetheless, it is also possible that aerobic methane oxidation has a greater influence than suggested by the model. Either way, both aerobic and anaerobic CH_4 oxidation have the potential to reduce GHG emissions at location C.

Both profiles C and E have an additional MOZ deeper down where all electron acceptors were already consumed. In profile C it looks like the slope changes in the lower part of the profile are due to an overfitting of the model to fluctuating concentrations within the methanogenic zone. In profile D however, the deepest MOZ is located where CH_4 oxidation would be expected, because of a clear slope change of the CH_4 concentration gradient. Potential electron acceptors could be SO_4^{2-}, which is present only few centimeters above, Fe- or Mn-oxides or perhaps trace amounts of O_2.

3.5 Microbial communities at location C

The relative abundance of 16S rRNA gene sequences with similarity to known methanogenic microbial groups increased with sediment depth into the methane zone (Fig. 6a). In the shallower depths (0-4 cm) the methanogenic microbial community was dominated by the Methanomasiliicoccales and Methanofastidiosales, whereas at the bottom of the profile (16-21 cm) Methanomethyliales and Methanomasiliicoccales dominated the methanogenic microbial community (Fig. 6b). The Methanomasiliicoccales and the Methanomethyliales both exhibit metabolic pathways in the genome indicative of H_2-dependent methylotrophic methanogenesis (Berghuis et al., 2019; Vanwonterghem et al., 2016). In saline or sulfate-rich environments, where methylated compounds like trimethyl amine or dimethyl sulfide are available as non-competitive substrates, this pathway can be of high importance (Conrad, 2020), but it is less considered in freshwater environments. However, Methanomassiliicoccales have been linked to CH_4 production from methanol in freshwater wetlands (Narrowe et al., 2019). Methanol can be derived from pectin which is contained in terrestrial plants (Conrad, 2005) and thus, the combination of a high relative abundance of Methanomassiliicoccales combined with a high input of allochthonous plant material found in the sediment cores render this production pathway possible. The strong depletion in $\delta^{13}C$-CH_4 in the methanogenic zone supports the potential for CH_4 production from methanol. Carbon fractionation factors related to CH_4 production from methanol (ε_C = 68-77) are similar to those of hydrogenotrophic methanogenesis (ε_C = 55-58) and much higher than for acetoclastic methanogenesis (ε_C = 24-27) or CH_4 production from other methylated compounds (Whiticar, 1999). The Methanomethyliales are a newly discovered group of methanogenic archaea branching within the Verstraetearchaeota (Berghuis et al., 2019; Vanwonterghem et al., 2016). The increased relative abundance of the Methanomethyliales in our sediment-core within the methane zone is a first clear evidence that these novel methanogenic archaea could be important for CH_4 production in the HZ.

Above the methane zone, there is an increased relative abundance of both aerobic and anaerobic CH_4 oxidizing microbial groups (Fig. 6d and e). The aerobic groups affiliated with Methylomonaceae (Gammaproteobacteria) and Methyloligellaceae (Alphaproteobacteria) dominated at depths above 12 cm (Fig. 6d), and are known to be involved in aerobic CH_4 oxidation (Takeuchi et al., 2019).

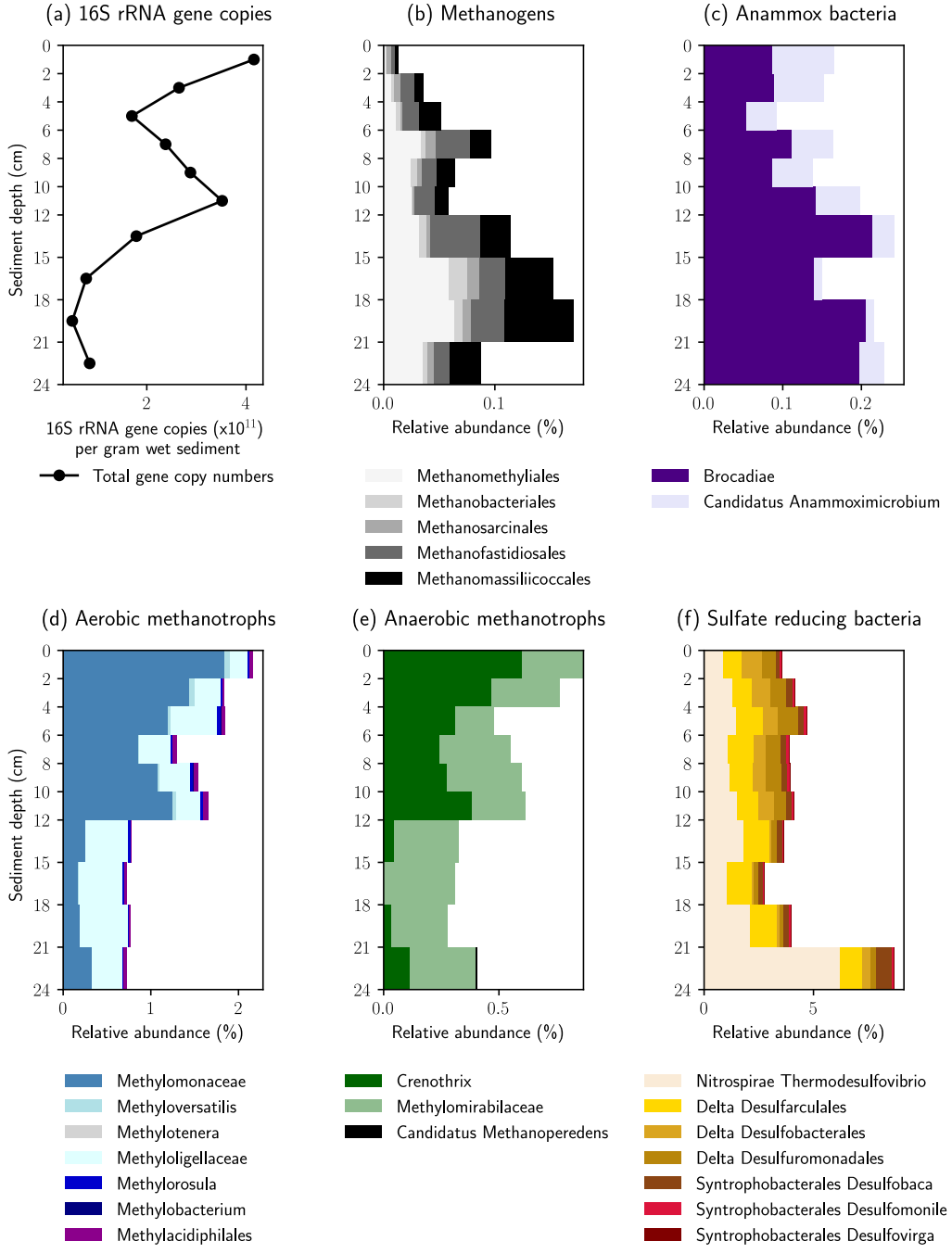

Figure 6: Relative abundance of key microbial groups detected in the 16S rRNA gene sequencing datasets. The histograms display the relative abundance (% of total reads) assigned to each group displayed. Note the increase in relative abundance of methanogenic groups below 12 cm, whereas the relative abundance of methane oxidizing groups increases above 12 cm.

The anaerobic methanotrophs had closest affiliation to *Methylomirabiliceae* and *Crenothrix*. Both are involved in different steps of coupling CH_4 oxidation to the reduction of NO_3^- and NO_2^- (Oswald et al., 2017; Ettwig et al., 2010). The results indicate that that anaerobic and aerobic CH_4 oxidizers can somehow inhabit the same sediment depths in the HZ, a finding that has been observed in paddy soil previously (Vaksmaa et al., 2017). *Crenothrix* are known to be facultative anaerobes, which can explain their presence in oxic environments, but O_2 was shown to have a detrimental effect on members of the *Methylomirabiliceae* like *Candidatus* Methylomirabilis oxyfera (Luesken et al., 2012). Their high abundance in the uppermost centimeters of the sediment is, therefore, surprising. Yet, the close proximity and co-existence of aerobic and anaerobic CH_4 oxidizers fits well to the observed steep and partly overlapping gradients. The mixed distribution of strict anaerobes together with aerobes and facultative aerobes within the HZ could be due to mixing and turbidity at the stream bottom, which might resuspend and distribute sediments to different zones.

The presence of 16S rRNA gene sequences affiliated with the bacterial groups Brocadiae and '*Candidatus* Anammoximicrobium' that are known to perform anaerobic oxidation of ammonium (Anammox) (Wu et al., 2020), may show that Anammox via nitrite reduction was also ongoing. Because the Anammox bacteria overlapped with anaerobic CH_4 oxidizing bacteria (*Methylomirabiliceae* and *Crenothrix)* in the vertical profile, our results might show that, similar to anoxic lake bottom water (Einsiedl et al., 2020), a coupling of Anammox with NO_2^- dependent CH_4 oxidation (N-DAMO) is possible in the anoxic sediments of the HZ. This may represent a mechanism whereby N_2 is released, and nitrogen is eliminated from the HZ. Based on the low abundance of ANME archaea we postulate that S-DAMO is unlikely to be a relevant process within the HZ of Moosach river. This is also in line with earlier findings by Shen et al. (2019) who found that NO_3^- and NO_2^- could trigger AOM in all sandy river sediments in their study, while SO_4^{2-} and Fe were only effective in a few examples

5 Conclusions

Measurements and interpretation of geochemical profiles and stable isotopes ($\delta^{13}C$-CH_4) at five different sampling sites in the river Moosach showed a predominant source of dissolved CH_4 and a potential for AOM. Based on our field study we confirm previous findings that large quantities of CH_4 are produced in river sediments, which can contribute to global warming. CH_4 was produced in all sampled locations, but CH_4 concentrations varied drastically between profiles. Much more CH_4 was produced in summer, especially in areas with fine, organic rich sediments like inside bends of curved river sections. These findings suggest that main influencing factors for CH_4 production in the HZ are temperature, organic carbon content and sediment composition. The uniqueness of the measured profiles underlines the high spatiotemporal variability in the hyporheic zone. Therefore, deriving general conclusions from point measurements is highly problematic and the representativeness of the available data should be critically questioned in future research on CH_4 emissions from rivers.

Based on measured $\delta^{13}C$ values and the microbial community found in location C, we consider hydrogenotrophic and H_2-dependent methylotrophic methanogenesis as relevant CH_4 production pathways. CH_4 concentrations at the sediment surface have been found to be low and $\delta^{13}C$-CH_4 values were almost constant over the sampled sediment depth in most of the measured

profiles, indicating a diffusion-limited transport of this GHG towards and across the sediment-water interface. However, in one of the profiles, an isotopic shift in $\delta^{13}C\text{-}CH_4$ to less negative values linked with decreasing CH_4 concentrations implied biological methane oxidation. Both microbiological and modeling methods showed the potential for anaerobic methane oxidation coupled with denitrification (N-DAMO). Yet, chemical gradients were very steep so that aerobic and anaerobic redox zones were in too close proximity to find a clear evidence for N-DAMO within the HZ of river Moosach. Nevertheless, our results clearly show the removal of nitrogen and decreasing CH_4 concentrations towards the sediment-water interface. Both processes are crucial in improving the quality of river water and in reducing GHG emissions to the atmosphere.

Appendix A: Surface water chemistry, sampling details and sediment characteristics

Table A1 shows the surface water chemistry of the Moosach river. The water is of calcium-magnesium-bicarbonate type with elevated chloride concentrations.

Table A1: Surface water chemistry. Concentrations represent mean values of data recorded between 2010-2018. Data retreived from the Bavarian State Office of the Environment.

Component	**Concentration** (mg L^{-1})
Na^+	30.9
Ca^{2+}	100
Mg^{2+}	20.7
Cl^-	54
NO_3^-	20.4
SO_4^{2-}	30.4
HCO_3^-	340
Dissolved O_2	8.7
TOC	3.5
DOC	2.8

Table A2 summarizes information on sampling intervals and measured basic chemical parameters of the surface water as measured on the days of sampling. Further, average discharge and temperature during equilibration period are given.

Table A2: Background information on the five sampling periods, basic chemical parameters of the surface water on the days of sampling and mean discharge and surface water temperature during the sampling period.

Profile	**Placement**	**Sampling**	**Days**	**Basic chemical parameters of the surface water on the days of sampling**				**Mean discharge & temperature during equilibration***	
				T_{SW} (° C)	**O_2** (mg L^{-1})	**pH**	**Conductivity** (µS cm^{-1})	**Q_M** (m^3 s^{-1})	**T_M** (° C)
A	02.03.2021	22.03.2021	36	7.0	no measurements			2.33	7.5
B	04.05.2021	26.05.2021	22	11.3	9.9	7.9	819	2.51	12.0
C	16.06.2021	06.07.2021	20	15.3	10.5	8.1	806	2.93	16.6
D	15.07.2020	20.08.2020	20	16.2	10.2	7.6	756	1.46	17.1
E	21.07.2021	18.08.2021	28	14.5	10.9	8.1	797	2.48	15.8

*Data retrieved from the Bavarian State Office of the Environment.

Sediment cores were taken at each sampling site by manually pushing a coring tube (inner diameter 42 mm) into the sediment. In the laboratory, each core was divided into homogeneous layers. Sieve-slurry analyses were performed to obtain sediment grain size distributions according to DIN EN ISO 17892-4. Sedimentation experiments failed for location B (11-22 cm) due to the high content of organic matter which induced coagulation at an unexpectedly high rate. Sedimentation experiments were not performed for location E 0-7 cm. The grain size distribution curves for each sampling site are displayed in Fig. A1 and characteristic values listed in Tab. A2.

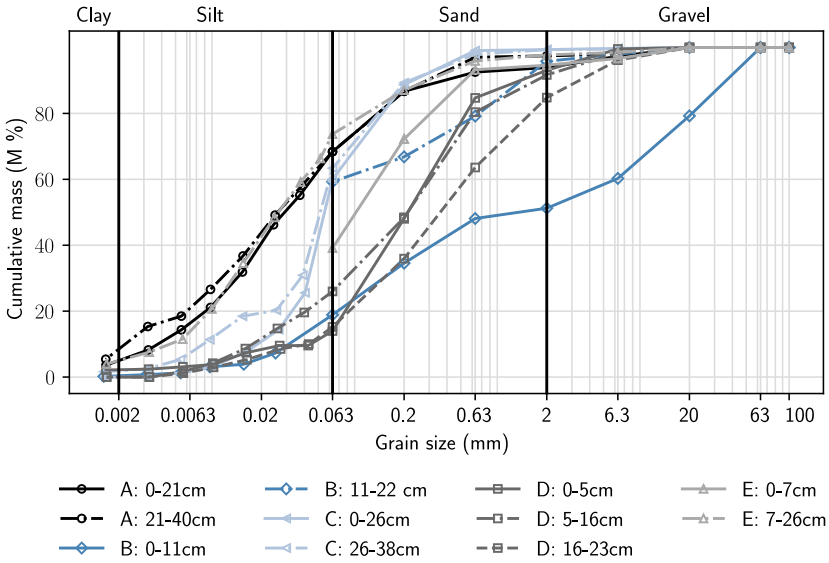

Figure A1: Grain size distribution curves

Porosity φ was calculated as a function of the median grain diameter d_{50} as suggested by Wu and Wang (2006) who modified the formula for initial porosity of sediment deposits (less than one year after deposition) proposed by Komura and Colby (1963). Values for d_{50} and φ are also given in Tab. A2. For location B (11-22 cm), the given d_{50} is an estimation based exclusively on the sieving analysis.

$$\varphi = 0.13 + \frac{0.21}{(d_{50}+0.002)^{0.21}} \quad \text{(A1)}$$

Table A3: Sediment characteristics and calculated porosity φ

Profile	**Sampling date**	**Depth** (cm)	**Silt/Clay** (%)	**Sand** (%)	**Gravel** (%)	$\mathbf{d_{50}}$ (mm)	**φ**
A	22.03.2021	0-21	65	29	6	0.030	0.56
		21-40	68	29	3	0.026	0.57
B	26.05.2021	0-11	19	32	49	1.46	0.32
		11-22	59	37	4	0.040	0.54
C	06.07.2021	0-26	60	39	1	0.030	0.51
		26-38	63	36	1	0.019	0.51
D	20.08.2020	0-5	14	79	7	0.22	0.42
		5-16	26	66	8	0.22	0.42
		16-23	15	70	15	0.42	0.38
E	18.08.2021	0-7	39	56	5	0.11	0.46
		7-26	74	24	2	0.027	0.57

Hydraulic conductivity K was roughly estimated using the formula introduced by Beyer (1964) (Eq. A2).

$$K = \beta \frac{g}{\nu} log\left(\frac{500}{C_U}\right) d_{10}^2 \quad \text{(A2)}$$

with the coefficient $\beta = 1.30 \cdot 10^{-5}$ as recommended by Rosas et al. (2014) for river sediments, the gravitational constant $g = 9.81\ m\ s^{-2}$, the kinematic viscosity $\nu = 1.307\ mm^2\ s^{-1}$ for 10 °C (Kestin et al., 1978), the uniformity coefficient $C_U = d_{60}/d_{10}$ and the grain diameters d_{10} and d_{60} at 10 % and 60 % of the cumulative grain size distribution curve, respectively. For location B (11-22 cm) and location E (0-7 cm) the d_{10} was estimated only based on the sieving analysis.

Table A4: Hydraulic conductivities estimated using the Beyer equation.

Profile	**Sampling date**	**Depth** (cm)	$\mathbf{d_{10}}$ (mm)	$\mathbf{d_{60}}$ (mm)	$\mathbf{C_U}$	**K** ($m\ s^{-1}$)
A	22.03.2021	0-21	0.0039	0.047	12.0	$2.4 \cdot 10^{-6}$
		21-40	0.0023	0.043	18.7	$7.4 \cdot 10^{-7}$
B	26.05.2021	0-11	0.041	6.2	150.5	$8.6 \cdot 10^{-5}$
		11-22	0.010	0.076	7.6	$1.8 \cdot 10^{-5}$
C	06.07.2021	0-26	0.0019	0.063	33.2	$4.1 \cdot 10^{-7}$
		26-38	0.008	0.062	7.8	$1.1 \cdot 10^{-5}$
D	20.08.2020	0-5	0.048	0.34	7.1	$4.2 \cdot 10^{-4}$
		5-16	0.018	0.36	20.0	$4.4 \cdot 10^{-5}$
		16-23	0.043	0.57	13.3	$2.8 \cdot 10^{-4}$
E	18.08.2021	0-7	0.020	0.15	7.5	$7.1 \cdot 10^{-5}$
		7-26	0.0047	0.039	8.3	$3.8 \cdot 10^{-6}$

Appendix B: Determination of a cut-off threshold concentration for isotope measurements

Measurements of δ^{13}C-CH_4 at low headspace CH_4 concentrations in the sample vials showed large standard deviations between repeated measurements. Thus, an experiment was conducted to find an appropriate cut-off value above which reliable isotopic data could be obtained. Two standards with -21.1 ‰ and -69.0 ‰ were diluted to obtain different concentrations and measured repeatedly. A cut-off value of 30 ppm was chosen based on the results displayed in Fig. B1.

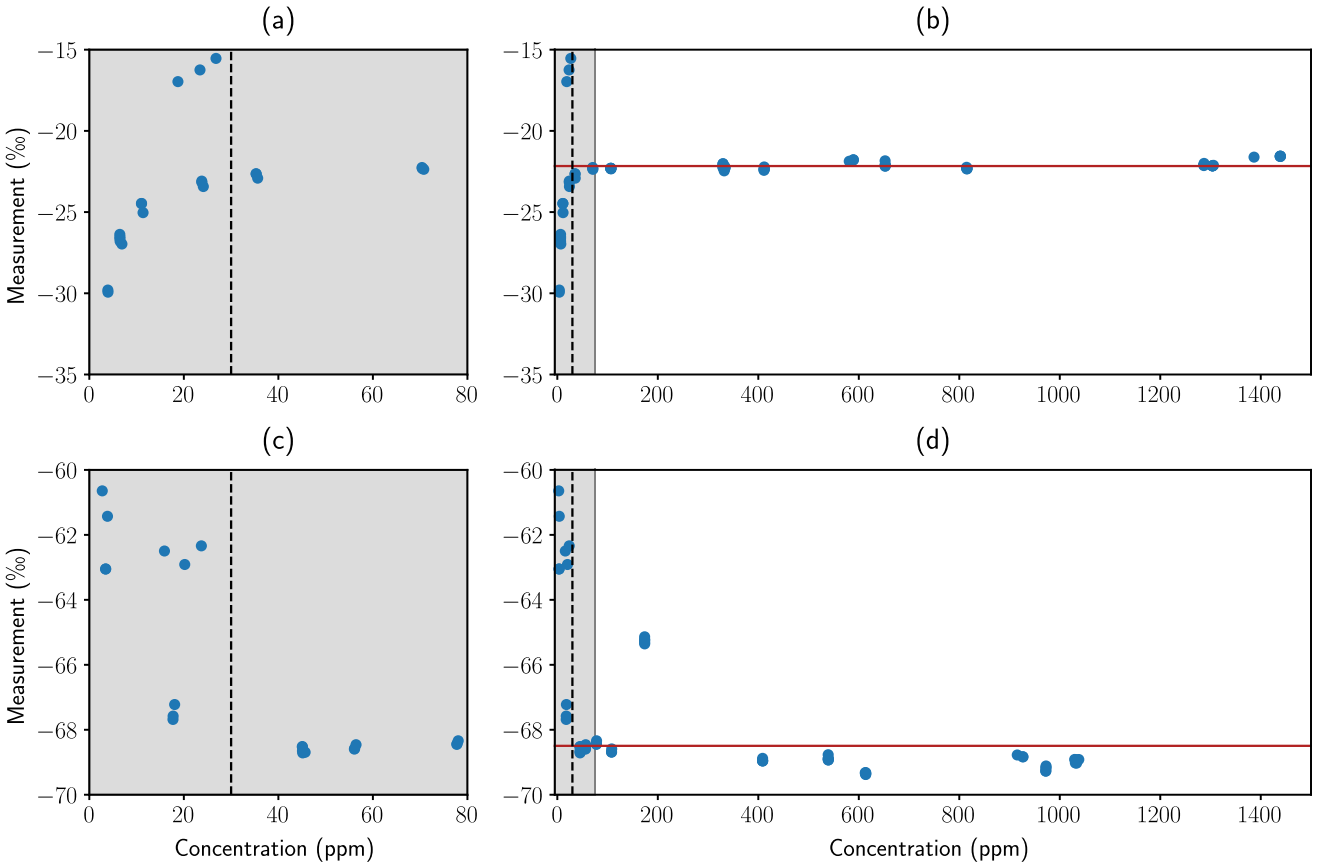

Figure B1: Repeated measurements of standards with δ^{13}C-CH_4 values of -21.1 ‰ (panels (a) and (b)) **and -69.0 ‰** (panels (c) and (d)). The red line in panels (b) and (d) represents the average value of all measurements above the cut-off threshold.

Appendix C: Calculation of sediment diffusion coefficients

Diffusion coefficients were calculated based on Boudreau (1997). Equations C1 and C2 have been used for the diffusion coefficients in water D^0 of gases and ions, respectively. The mean surface water temperature during the equilibration period of the peeper T_M (Tab. A2) was used for temperatures in Eq. C1 and C2.

$$D^0 = 4.72 \cdot 10^{-9} \frac{T}{\mu V_b^{0.6}} \quad \text{(C1)}$$

where μ is the dynamic viscosity of water in units of poise, T the absolute temperature [°K] and V_b the molar volume of the solute. Values for V_b are given in Tab. C1.

Table C1: Parameters for the calculation of D^0 in for relevant gases

Species	V_b
O_2	27.9
CH_4	37.7

$$D^0 = (m_0 + m_1 t) \cdot 10^{-6} \quad \text{(C2)}$$

where m_0 and m_1 are parameters listed in Tab. C2 and t is temperature in [°C].

Table C2: Parameters for the calculation of D^0 for relevant ions

Ion	m_0	m_1
NO_3^-	9.50	0.388
SO_4^{2-}	4.88	0.232

Table C3 shows diffusion coefficient for the different solutes and sampling dates in water and Tab. C4 the calculated sediment diffusion coefficients based on the Eq. C3 (Iversen and Jørgensen, 1993).

$$D_S = \frac{D^0}{1+3(1-\varphi)} \quad \text{(C3)}$$

where D_S is the diffusion coefficient in the sediment, D^0 the temperature-dependent diffusion coefficient in water and φ the porosity.

665 **Table C3: Calculated values for D^0 for mean surface water temperature during the sampling period T_M**

Profile	**Sampling date**	T_M (°C)	D^0_{CH4} (x 10^{-5} cm^2 s^{-1})	D^0_{O2} (x 10^{-5} cm^2 s^{-1})	D^0_{NO3} (x 10^{-5} cm^2 s^{-1})	D^0_{SO4} (x 10^{-6} cm^2 s^{-1})
A	22.03.2021	7.4	1.04	1.25	1.22	6.50
B	26.05.2021	11.3	1.20	1.44	1.39	7.50
C	06.07.2021	15.3	1.36	1.63	1.54	8.43
D	20.08.2020	16.2	1.40	1.67	1.58	8.64
E	18.08.2021	14.5	1.33	1.59	1.51	8.24

Table C4: Calculated values for D_S for sampling days and sedimentary layers

Profile	**Sampling date**	**Sediment depth** (cm)	φ	$D_{S,CH4}$ (x 10^{-6} cm^2 s^{-1})	$D_{S,O2}$ (x 10^{-6} cm^2 s^{-1})	$D_{S,NO3}$ (x 10^{-6} cm^2 s^{-1})	$D_{S,SO4}$ (x 10^{-6} cm^2 s^{-1})
A	22.03.2021	0-21	0.56	4.50	5.39	5.27	2.80
		21-40	0.57	4.56	5.46	5.33	2.84
B	26.05.2021	0-11	0.32	3.99	4.75	4.57	2.47
		11-22	0.54	5.09	6.06	5.83	3.15
C	06.07.2021	0-26	0.51	5.53	6.62	6.25	3.41
D	20.08.2020	0-16	0.42	5.10	6.12	5.76	3.15
		16-23	0.38	4.89	5.86	5.52	3.02
E	18.08.2021	0-7	0.46	5.08	6.09	5.77	3.15
		7-26	0.57	5.81	6.97	6.61	3.60

Appendix D: Correlation between CH_4 and NH_4^+ data

Figure D1 shows the correlation between CH_4 and NH_4^+ concentrations. In profile A, no NH_4^+ could be detected, therefore only data for profiles B-E is displayed. A clear positive linear correlation can be observed for profiles C and D. In profile B, NH_4^+ was mostly below the detection limit of 0.005 mmol L^{-1}. Higher concentrations were only found between 6-14 cm depth, above the zone where CH_4 concentrations peaked (increased CH_4 concentrations between 5-23 cm depth with a peak at 15 cm depth). A negative correlation between CH_4 and NH_4^+ concentrations appears to exist between 6-14 cm depth. In profile E, no correlation can be observed, NH_4^+ concentrations are generally very low compared to the other profiles.

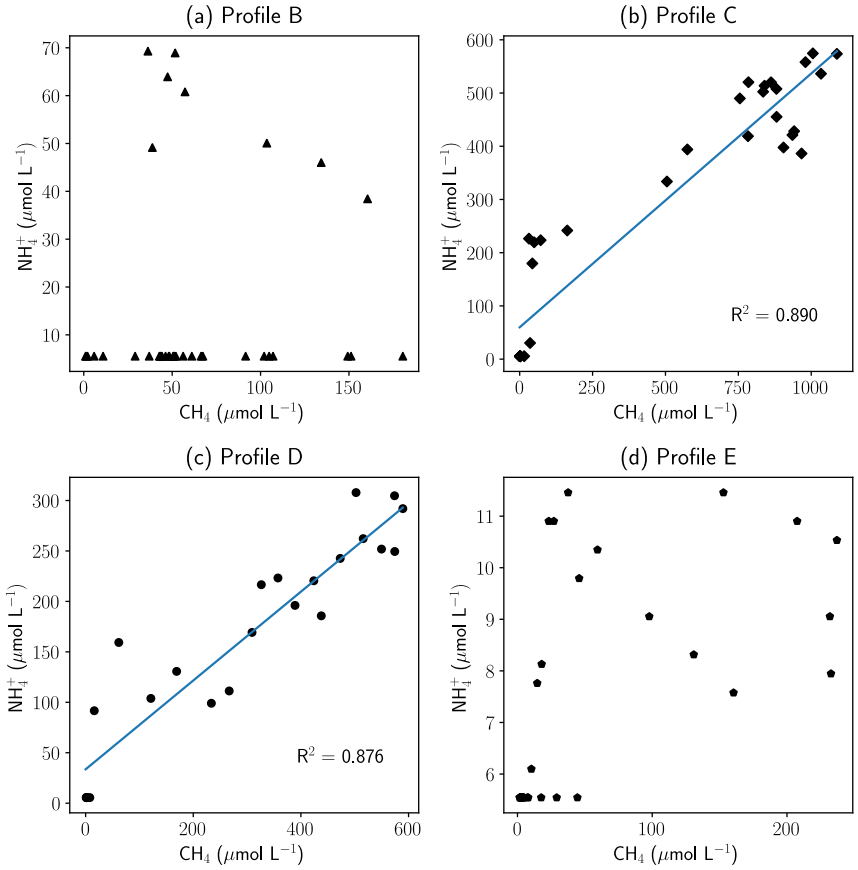

Figure D1: Correlation between CH_4 and NH_4^+. Each panel corresponds to one measured profile. Axes are scaled in the range of the data. For profiles C and D, a linear regression was performed and R^2 values are given in the respective plots. Panels (a) to (d) correspond to profiles B-E, respectively.

Author contributions

TM, AW and FE conceptualized the project. TM and AW developed the methodology and performed field works. ÖC and WO contributed the microbiological investigations. TM was responsible for visualization and original draft preparation. Funding acquisition and supervision were performed by FE and TB. TM, AW, WO, TB and FE all participated in writing, review and editing.

Competing interests

The authors declare that they have no competing interests.

Acknowledgements

We thank Tobias Lanzl for support during the field campaign as well as Susanne Thiemann and Jaroslava Obel for their help with analytics in the laboratory. We also want to thank Dr. Friedhelm Pfeiffer for critical reading and reviewing. Further, we want to acknowledge the good cooperation with the team of the Chair of Systems Biology (TUM).

References

Arshad, A., Speth, D. R., de Graaf, R. M., Op den Camp, H. J., Jetten, M. S., and Welte, C. U.: A metagenomics-based metabolic model of nitrate-dependent anaerobic oxidation of methane by Methanoperedens-like archaea, Front Microbiol, 6, 1423, 2015.

Auerswald, K. and Geist, J.: Extent and causes of siltation in a headwater stream bed: catchment soil erosion is less important than internal stream processes, Land Degradation & Development, 29, 737-748, 2018.

Bardini, L., Boano, F., Cardenas, M., Revelli, R., and Ridolfi, L.: Nutrient cycling in bedform induced hyporheic zones, Geochimica et Cosmochimica Acta, 84, 47-61, 2012.

Bardini, L., Boano, F., Cardenas, M., Sawyer, A., Revelli, R., and Ridolfi, L.: Small-scale permeability heterogeneity has negligible effects on nutrient cycling in streambeds, Geophys Res Lett, 40, 1118-1122, 2013.

Bavarian State Office of the Environment. Gewässerkundlicher Dienst Bayern: https://www.gkd.bayern.de/en/, last access: 19.01.2022.

Beal, E. J., House, C. H., and Orphan, V. J.: Manganese-and iron-dependent marine methane oxidation, Science, 325, 184-187, 2009.

Bednařík, A., Blaser, M., Matoušů, A., Tušer, M., Chaudhary, P. P., Šimek, K., and Rulík, M.: Sediment methane dynamics along the Elbe River, Limnologica, 79, 125716, 2019.

Berg, P., Risgaard-Petersen, N., and Rysgaard, S.: Interpretation of measured concentration profiles in sediment pore water, Limnol Oceanogr, 43, 1500-1510, 1998.

Berghuis, B. A., Yu, F. B., Schulz, F., Blainey, P. C., Woyke, T., and Quake, S. R.: Hydrogenotrophic methanogenesis in archaeal phylum Verstraetearchaeota reveals the shared ancestry of all methanogens, Proceedings of the National Academy of Sciences, 116, 5037-5044, 2019.

Beyer, W.: Zur bestimmung der wasserdurchlässigkeit von kiesen und sanden aus der kornverteilungskurve, WWT, 14, 165-168, 1964.

Boano, F., Harvey, J. W., Marion, A., Packman, A. I., Revelli, R., Ridolfi, L., and Wörman, A.: Hyporheic flow and transport processes: Mechanisms, models, and biogeochemical implications, Reviews of Geophysics, 52, 603-679, 2014.

Bodmer, P., Wilkinson, J., and Lorke, A.: Sediment properties drive spatial variability of potential methane production and oxidation in small streams, Journal of Geophysical Research: Biogeosciences, 125, e2019JG005213, 2020.

Borges, A. V., Darchambeau, F., Teodoru, C. R., Marwick, T. R., Tamooh, F., Geeraert, N., Omengo, F. O., Guérin, F., Lambert, T., and Morana, C.: Globally significant greenhouse-gas emissions from African inland waters, Nature Geoscience, 8, 637-642, 2015.

Boudreau, B. P.: Diagenetic models and their implementation, Springer, Berlin1997.

Braun, A., Auerswald, K., and Geist, J.: Drivers and spatio-temporal extent of hyporheic patch variation: implications for sampling, 2012.

Canfield, D. E. and Thamdrup, B.: Towards a consistent classification scheme for geochemical environments, or, why we wish the term ‘suboxic’would go away, Geobiology, 7, 385-392, 2009.

Capone, D. G. and Kiene, R. P.: Comparison of microbial dynamics in marine and freshwater sediments: Contrasts in anaerobic carbon catabolism 1, Limnol Oceanogr, 33, 725-749, 1988.

Casagrande, D. J., Siefert, K., Berschinski, C., and Sutton, N.: Sulfur in peat-forming systems of the Okefenokee Swamp and Florida Everglades: origins of sulfur in coal, Geochimica et Cosmochimica Acta, 41, 161-167, 1977.

Comer-Warner, S. A., Romeijn, P., Gooddy, D. C., Ullah, S., Kettridge, N., Marchant, B., Hannah, D. M., and Krause, S.: Thermal sensitivity of CO 2 and CH 4 emissions varies with streambed sediment properties, Nat Commun, 9, 1-9, 2018.

Conrad, R.: Quantification of methanogenic pathways using stable carbon isotopic signatures: a review and a proposal, Org Geochem, 36, 739-752, 2005.

Conrad, R.: Importance of hydrogenotrophic, aceticlastic and methylotrophic methanogenesis for methane production in terrestrial, aquatic and other anoxic environments: a mini review, Pedosphere, 30, 25-39, 2020.

Coskun, Ö. K., Özen, V., Wankel, S. D., and Orsi, W. D.: Quantifying population-specific growth in benthic bacterial communities under low oxygen using H218O, The ISME journal, 13, 1546-1559, 2019.

Crawford, J. T., Loken, L. C., West, W. E., Crary, B., Spawn, S. A., Gubbins, N., Jones, S. E., Striegl, R. G., and Stanley, E. H.: Spatial heterogeneity of within-stream methane concentrations, Journal of Geophysical Research: Biogeosciences, 122, 1036-1048, 2017.

Danczak, R. E., Sawyer, A. H., Williams, K. H., Stegen, J. C., Hobson, C., and Wilkins, M. J.: Seasonal hyporheic dynamics control coupled microbiology and geochemistry in Colorado River sediments, Journal of Geophysical Research: Biogeosciences, 121, 2976-2987, 2016.

DelSontro, T., McGinnis, D. F., Sobek, S., Ostrovsky, I., and Wehrli, B.: Extreme Methane Emissions from a Swiss Hydropower Reservoir: Contribution from Bubbling Sediments, Environ Sci Technol, 44, 2419-2425, 10.1021/es9031369, 2010.

Deppenmeier, U.: The unique biochemistry of methanogenesis, Progress in Nucleic Acid Research and Molecular Biology, 71, 223-283, 2002.

Deutzmann, J. S., Stief, P., Brandes, J., and Schink, B.: Anaerobic methane oxidation coupled to denitrification is the dominant methane sink in a deep lake, Proceedings of the National Academy of Sciences, 111, 18273-18278, 10.1073/pnas.1411617111, 2014.

Edgar, R. C.: UPARSE: highly accurate OTU sequences from microbial amplicon reads, Nature methods, 10, 996-998, 2013.

Einsiedl, F., Wunderlich, A., Sebilo, M., Coskun, Ö. K., Orsi, W. D., and Mayer, B.: Biogeochemical evidence of anaerobic methane oxidation and anaerobic ammonium oxidation in a stratified lake using stable isotopes, Biogeosciences, 17, 5149-5161, 2020.

Eller, G., Känel, L., and Krüger, M.: Cooccurrence of aerobic and anaerobic methane oxidation in the water column of Lake Plußsee, Appl Environ Microb, 71, 8925-8928, 2005.

EPA: Technical Guidance for the Natural Attenuation Indicators: Methane, Ethane, and Ethene, 2001.

Ettwig, K. F., Butler, M. K., Le Paslier, D., Pelletier, E., Mangenot, S., Kuypers, M. M., Schreiber, F., Dutilh, B. E., Zedelius, J., and de Beer, D.: Nitrite-driven anaerobic methane oxidation by oxygenic bacteria, Nature, 464, 543-548, 2010.

European Commission and United States of America: Global Methane Pledge, Climate and Clean Air Coalition, 2, 2021.

Findlay, S.: Importance of surface-subsurface exchange in stream ecosystems: The hyporheic zone, Limnol Oceanogr, 40, 159-164, 1995.

Graf, J. S., Mayr, M. J., Marchant, H. K., Tienken, D., Hach, P. F., Brand, A., Schubert, C. J., Kuypers, M. M., and Milucka, J.: Bloom of a denitrifying methanotroph,'Candidatus Methylomirabilis limnetica', in a deep stratified lake, Environ Microbiol, 20, 2598-2614, 2018.

Haroon, M. F., Hu, S., Shi, Y., Imelfort, M., Keller, J., Hugenholtz, P., Yuan, Z., and Tyson, G. W.: Anaerobic oxidation of methane coupled to nitrate reduction in a novel archaeal lineage, Nature, 500, 567-570, 10.1038/nature12375, 2013.

Hesslein, R. H.: An in situ sampler for close interval pore water studies 1, Limnol Oceanogr, 21, 912-914, 1976.

Hu, B.-l., Shen, L.-d., Lian, X., Zhu, Q., Liu, S., Huang, Q., He, Z.-f., Geng, S., Cheng, D.-q., Lou, L.-p., Xu, X.-y., Zheng, P., and He, Y.-f.: Evidence for nitrite-dependent anaerobic methane oxidation as a previously overlooked microbial methane sink in wetlands, Proceedings of the National Academy of Sciences, 111, 4495-4500, 10.1073/pnas.1318393111, 2014.

IPCC: The physical science basis, Cambridge, United Kingdom and New York, NY, USA, 2013.

Iversen, N. and Jørgensen, B. B.: Diffusion coefficients of sulfate and methane in marine sediments: Influence of porosity, Geochimica et Cosmochimica Acta, 57, 571-578, 1993.

Jørgensen, B. B., Weber, A., and Zopfi, J.: Sulfate reduction and anaerobic methane oxidation in Black Sea sediments, Deep Sea Research Part I: Oceanographic Research Papers, 48, 2097-2120, 2001.

Kampbell, D. H. and Vandegrift, S. A.: Analysis of dissolved methane, ethane, and ethylene in ground water by a standard gas chromatographic technique, Journal of Chromatographic Science, 36, 253-256, 1998.

Kestin, J., Sokolov, M., and Wakeham, W. A.: Viscosity of liquid water in the range− 8 C to 150 C, Journal of Physical and Chemical Reference Data, 7, 941-948, 1978.

Kirschke, S., Bousquet, P., Ciais, P., Saunois, M., Canadell, J. G., Dlugokencky, E. J., Bergamaschi, P., Bergmann, D., Blake, D. R., and Bruhwiler, L.: Three decades of global methane sources and sinks, Nature geoscience, 6, 813-823, 2013.

Kits, K. D., Klotz, M. G., and Stein, L. Y.: Methane oxidation coupled to nitrate reduction under hypoxia by the G ammaproteobacterium M ethylomonas denitrificans, sp. nov. type strain FJG1, Environ Microbiol, 17, 3219-3232, 2015.

Komura, S. and Colby, B. R.: Sediment Transportation Mechanics: Introduction and Properties of Sediment, Journal of the Hydraulics Division, 89, 263-268, 1963.

Krzycki, J., Kenealy, W., DeNiro, M., and Zeikus, J.: Stable carbon isotope fractionation by Methanosarcina barkeri during methanogenesis from acetate, methanol, or carbon dioxide-hydrogen, Appl Environ Microb, 53, 2597-2599, 1987.

Ladd, J. and Jackson, R.: Biochemistry of ammonification, Nitrogen in agricultural soils, 22, 173-228, 1982.

Luesken, F. A., Wu, M. L., Op den Camp, H. J., Keltjens, J. T., Stunnenberg, H., Francoijs, K. J., Strous, M., and Jetten, M. S.: Effect of oxygen on the anaerobic methanotroph 'Candidatus Methylomirabilis oxyfera': kinetic and transcriptional analysis, Environ Microbiol, 14, 1024-1034, 2012.

Mach, V., Blaser, M. B., Claus, P., Chaudhary, P. P., and Rulík, M.: Methane production potentials, pathways, and communities of methanogens in vertical sediment profiles of river Sitka, Front Microbiol, 6, 506, 2015.

Marzadri, A., Tonina, D., and Bellin, A.: Morphodynamic controls on redox conditions and on nitrogen dynamics within the hyporheic zone: Application to gravel bed rivers with alternate-bar morphology, Journal of Geophysical Research: Biogeosciences, 117, 2012.

McGinnis, D. F., Bilsley, N., Schmidt, M., Fietzek, P., Bodmer, P., Premke, K., Lorke, A., and Flury, S.: Deconstructing methane emissions from a small Northern European river: Hydrodynamics and temperature as key drivers, Environ Sci Technol, 50, 11680-11687, 2016.

Naqvi, S. W. A., Lam, P., Narvenkar, G., Sarkar, A., Naik, H., Pratihary, A., Shenoy, D. M., Gauns, M., Kurian, S., and Damare, S.: Methane stimulates massive nitrogen loss from freshwater reservoirs in India, Nat Commun, 9, 1-10, 2018.

Narrowe, A. B., Borton, M. A., Hoyt, D. W., Smith, G. J., Daly, R. A., Angle, J. C., Eder, E. K., Wong, A. R., Wolfe, R. A., and Pappas, A.: Uncovering the diversity and activity of methylotrophic methanogens in freshwater wetland soils, Msystems, 4, e00320-00319, 2019.

Nazaries, L., Murrell, J. C., Millard, P., Baggs, L., and Singh, B. K.: Methane, microbes and models: fundamental understanding of the soil methane cycle for future predictions, Environ Microbiol, 15, 2395-2417, 2013.

Ng, G. H. C., Rosenfeld, C. E., Santelli, C. M., Yourd, A. R., Lange, J., Duhn, K., and Johnson, N. W.: Microbial and reactive transport modeling evidence for hyporheic flux-driven cryptic sulfur cycling and anaerobic methane oxidation in a sulfate-impacted wetland-stream system, Journal of Geophysical Research: Biogeosciences, 125, e2019JG005185, 2020.

Nisbet, E. G., Manning, M., Dlugokencky, E., Fisher, R., Lowry, D., Michel, S., Myhre, C. L., Platt, S. M., Allen, G., and Bousquet, P.: Very strong atmospheric methane growth in the 4 years 2014–2017: Implications for the Paris Agreement, Global Biogeochemical Cycles, 33, 318-342, 2019.

Norði, K. á. and Thamdrup, B.: Nitrate-dependent anaerobic methane oxidation in a freshwater sediment, Geochimica et Cosmochimica Acta, 132, 141-150, 2014.

Norði, K. á., Thamdrup, B., and Schubert, C. J.: Anaerobic oxidation of methane in an iron-rich Danish freshwater lake sediment, Limnol Oceanogr, 58, 546-554, 2013.

Oswald, K., Graf, J. S., Littmann, S., Tienken, D., Brand, A., Wehrli, B., Albertsen, M., Daims, H., Wagner, M., and Kuypers, M. M.: Crenothrix are major methane consumers in stratified lakes, The ISME journal, 11, 2124-2140, 2017.

Parkhurst, D. L. and Appelo, C.: Description of input and examples for PHREEQC version 3 - a computer program for speciation, batch-reaction, one-dimensional transport, and inverse geochemical calculations, US geological survey techniques and methods, 6, 497, 2013.

Peña Sanchez, A., Mayer, B., Wunderlich, A., Rein, A., and Einsiedl, F.: Analysing seasonal variations of methane oxidation processes coupled with denitrification in a stratified lake using stable isotopes and numerical modeling, Geochimica et Cosmochimica Acta, 2022.

Pichler, M., Coskun, Ö. K., Ortega-Arbulú, A. S., Conci, N., Wörheide, G., Vargas, S., and Orsi, W. D.: A 16S rRNA gene sequencing and analysis protocol for the Illumina MiniSeq platform, Microbiologyopen, 7, e00611, 2018.

Pulg, U., Barlaup, B. T., Sternecker, K., Trepl, L., and Unfer, G.: Restoration of spawning habitats of brown trout (Salmo trutta) in a regulated chalk stream, River Research and Applications, 29, 172-182, 2013.

Quast, C., Pruesse, E., Yilmaz, P., Gerken, J., Schweer, T., Yarza, P., Peplies, J., and Glöckner, F. O.: The SILVA ribosomal RNA gene database project: improved data processing and web-based tools, Nucleic acids research, 41, D590-D596, 2012.

Raghoebarsing, A. A., Pol, A., van de Pas-Schoonen, K. T., Smolders, A. J. P., Ettwig, K. F., Rijpstra, W. I. C., Schouten, S., Damsté, J. S. S., Op den Camp, H. J. M., Jetten, M. S. M., and Strous, M.: A microbial consortium couples anaerobic methane oxidation to denitrification, Nature, 440, 918-921, 10.1038/nature04617, 2006.

Reeburgh, W. S.: Methane consumption in Cariaco Trench waters and sediments, Earth Planet Sc Lett, 28, 337-344, 1976.

Romeijn, P., Comer-Warner, S. A., Ullah, S., Hannah, D. M., and Krause, S.: Streambed organic matter controls on carbon dioxide and methane emissions from streams, Environ Sci Technol, 53, 2364-2374, 2019.

Rosas, J., Lopez, O., Missimer, T. M., Coulibaly, K. M., Dehwah, A. H., Sesler, K., Lujan, L. R., and Mantilla, D.: Determination of hydraulic conductivity from grain-size distribution for different depositional environments, Groundwater, 52, 399-413, 2014.

Rutherford, J., Latimer, G., and Smith, R.: Bedform mobility and benthic oxygen uptake, Water Res, 27, 1545-1558, 1993.

Rutherford, J., Boyle, J., Elliott, A., Hatherell, T., and Chiu, T.: Modeling benthic oxygen uptake by pumping, Journal of Environmental Engineering, 121, 84-95, 1995.

Saunois, M., Stavert, A. R., Poulter, B., Bousquet, P., Canadell, J. G., Jackson, R. B., Raymond, P. A., Dlugokencky, E. J., Houweling, S., and Patra, P. K.: The global methane budget 2000–2017, Earth System Science Data, 12, 1561-1623, 2020.

Schubert, C. J., Vazquez, F., Lösekann-Behrens, T., Knittel, K., Tonolla, M., and Boetius, A.: Evidence for anaerobic oxidation of methane in sediments of a freshwater system (Lago di Cadagno), FEMS microbiology ecology, 76, 26-38, 2011.

Segarra, K., Schubotz, F., Samarkin, V., Yoshinaga, M., Hinrichs, K., and Joye, S.: High rates of anaerobic methane oxidation in freshwater wetlands reduce potential atmospheric methane emissions, Nat Commun, 6, 1-8, 2015.

Shelley, F., Abdullahi, F., Grey, J., and Trimmer, M.: Microbial methane cycling in the bed of a chalk river: oxidation has the potential to match methanogenesis enhanced by warming, Freshwater Biology, 60, 150-160, 2015.

Shelley, F., Ings, N., Hildrew, A. G., Trimmer, M., and Grey, J.: Bringing methanotrophy in rivers out of the shadows, Limnol Oceanogr, 62, 2345-2359, 2017.

Shen, L.-d., Ouyang, L., Zhu, Y., and Trimmer, M.: Active pathways of anaerobic methane oxidation across contrasting riverbeds, The ISME journal, 13, 752-766, 2019.

Shen, L.-d., Wu, H.-s., Liu, X., and Li, J.: Cooccurrence and potential role of nitrite-and nitrate-dependent methanotrophs in freshwater marsh sediments, Water Res, 123, 162-172, 2017.

Silvennoinen, H., Liikanen, A., Rintala, J., and Martikainen, P. J.: Greenhouse gas fluxes from the eutrophic Temmesjoki River and its Estuary in the Liminganlahti Bay (the Baltic Sea), Biogeochemistry, 90, 193-208, 2008.

Spoelstra, J., Leal, K. A., Senger, N. D., Schiff, S. L., and Post, R.: Isotopic characterization of sulfate in a shallow aquifer impacted by agricultural fertilizer, Groundwater, 59, 658-670, 2021.

Spratt Jr, H. G., Morgan, M. D., and Good, R. E.: Sulfate reduction in peat from a New Jersey pinelands cedar swamp, Appl Environ Microb, 53, 1406-1411, 1987.

Stanley, E. H., Casson, N. J., Christel, S. T., Crawford, J. T., Loken, L. C., and Oliver, S. K.: The ecology of methane in streams and rivers: patterns, controls, and global significance, Ecological Monographs, 86, 146-171, 10.1890/15-1027, 2016.

Storey, R., Fulthorpe, R. R., and Williams, D. D.: Perspectives and predictions on the microbial ecology of the hyporheic zone, Freshwater Biology, 41, 119-130, 1999.

Sunjidmaa, N., Mendoza-Lera, C., Hille, S., Schmidt, C., Borchardt, D., and Graeber, D.: Carbon limitation may override fine-sediment induced alterations of hyporheic nitrogen and phosphorus dynamics, Sci Total Environ, 837, 155689, https://doi.org/10.1016/j.scitotenv.2022.155689, 2022.

Takeuchi, M., Ozaki, H., Hiraoka, S., Kamagata, Y., Sakata, S., Yoshioka, H., and Iwasaki, W.: Possible cross-feeding pathway of facultative methylotroph Methyloceanibacter caenitepidi Gela4 on methanotroph Methylocaldum marinum S8, PloS one, 14, e0213535, 2019.

Teasdale, P. R., Batley, G. E., Apte, S. C., and Webster, I. T.: Pore water sampling with sediment peepers, TrAC Trends in Analytical Chemistry, 14, 250-256, 1995.

Timmers, P. H., Suarez-Zuluaga, D. A., van Rossem, M., Diender, M., Stams, A. J., and Plugge, C. M.: Anaerobic oxidation of methane associated with sulfate reduction in a natural freshwater gas source, The ISME journal, 10, 1400-1412, 2016.

Trimmer, M., Grey, J., Heppell, C. M., Hildrew, A. G., Lansdown, K., Stahl, H., and Yvon-Durocher, G.: River bed carbon and nitrogen cycling: state of play and some new directions, Sci Total Environ, 434, 143-158, 2012.

Triska, F. J., Duff, J. H., and Avanzino, R. J.: The role of water exchange between a stream channel and its hyporheic zone in nitrogen cycling at the terrestrial—aquatic interface, in: Nutrient dynamics and retention in land/water ecotones of lowland, temperate lakes and rivers, Springer, 167-184, 1993.

Vaksmaa, A., van Alen, T. A., Ettwig, K. F., Lupotto, E., Valè, G., Jetten, M. S., and Lüke, C.: Stratification of diversity and activity of methanogenic and methanotrophic microorganisms in a nitrogen-fertilized Italian paddy soil, Front Microbiol, 8, 2127, 2017.

van Grinsven, S., Sinninghe Damsté, J. S., Abdala Asbun, A., Engelmann, J. C., Harrison, J., and Villanueva, L.: Methane oxidation in anoxic lake water stimulated by nitrate and sulfate addition, Environ Microbiol, 22, 766-782, 2020.

Vanwonterghem, I., Evans, P. N., Parks, D. H., Jensen, P. D., Woodcroft, B. J., Hugenholtz, P., and Tyson, G. W.: Methylotrophic methanogenesis discovered in the archaeal phylum Verstraetearchaeota, Nature microbiology, 1, 1-9, 2016.

Vermaat, J. E., Harmsen, J., Hellmann, F. A., van der Geest, H. G., de Klein, J. J., Kosten, S., Smolders, A. J., Verhoeven, J. T., Mes, R. G., and Ouboter, M.: Annual sulfate budgets for Dutch lowland peat polders: The soil is a major sulfate source through peat and pyrite oxidation, Journal of Hydrology, 533, 515-522, 2016.

Versantvoort, W., Guerrero-Cruz, S., Speth, D. R., Frank, J., Gambelli, L., Cremers, G., van Alen, T., Jetten, M. S., Kartal, B., and Op den Camp, H. J.: Comparative genomics of Candidatus Methylomirabilis species and description of Ca. Methylomirabilis lanthanidiphila, Front Microbiol, 9, 1672, 2018.

Villa, J. A., Smith, G. J., Ju, Y., Renteria, L., Angle, J. C., Arntzen, E., Harding, S. F., Ren, H., Chen, X., and Sawyer, A. H.: Methane and nitrous oxide porewater concentrations and surface fluxes of a regulated river, Sci Total Environ, 715, 136920, 2020.

Vuillemin, A., Wankel, S. D., Coskun, Ö. K., Magritsch, T., Vargas, S., Estes, E. R., Spivack, A. J., Smith, D. C., Pockalny, R., and Murray, R. W.: Archaea dominate oxic subseafloor communities over multimillion-year time scales, Science Advances, 5, eaaw4108, 2019.

Whiticar, M. J.: Carbon and hydrogen isotope systematics of bacterial formation and oxidation of methane, Chemical Geology, 161, 291-314, 1999.

Whiticar, M. J., Faber, E., and Schoell, M.: Biogenic methane formation in marine and freshwater environments: CO2 reduction vs. acetate fermentation—isotope evidence, Geochimica et Cosmochimica Acta, 50, 693-709, 1986.

Winter, T. C., Harvey, J. W., Franke, L. O., and Alley, W. M.: Ground water and surface water: A single resource, U.S. Geological Survey, Denver, Colorado, 1998.

Wu, G., Zhang, T., Gu, M., Chen, Z., and Yin, Q.: Review of characteristics of anammox bacteria and strategies for anammox start-up for sustainable wastewater resource management, Water Sci Technol, 82, 1742-1757, 2020.

Wu, W. and Wang, S. S.: Formulas for sediment porosity and settling velocity, Journal of Hydraulic Engineering, 132, 858-862, 2006.

Zehlius-Eckert, W., Schwaiger, H., and Beckmann, A.: Monitoring und Erfolgskontrolle im Freisinger Moos,

Zhang, M., Luo, Y., Lin, X., Hetharua, B., Zhao, W., Zhou, M., Zhan, Q., Xu, H., Zheng, T., and Tian, Y.: Molecular and stable isotopic evidence for the occurrence of nitrite-dependent anaerobic methane-oxidizing bacteria in the mangrove sediment of Zhangjiang Estuary, China, Applied microbiology and biotechnology, 102, 2441-2454, 2018.

Zhu, G., Zhou, L., Wang, Y., Wang, S., Guo, J., Long, X. E., Sun, X., Jiang, B., Hou, Q., and Jetten, M. S.: Biogeographical distribution of denitrifying anaerobic methane oxidizing bacteria in C hinese wetland ecosystems, Environmental microbiology reports, 7, 128-138, 2015.

Zimmer, M. A. and Lautz, L. K.: Temporal and spatial response of hyporheic zone geochemistry to a storm event, Hydrological Processes, 28, 2324-2337, 2014.